Ultrasound-assisted synthesis of copper-based catalysts for the electrocatalytic CO2 reduction: Effect of ultrasound irradiation, precursor concentration and calcination

Sustainable Materials and Technologies 35 (2023) e00557

Contents lists available at ScienceDirect

Sustainable Materials and Technologies

journal homepage: www.elsevier.com/locate/susmat

Ultrasound-assisted synthesis of copper-based catalysts for the electrocatalytic CO_2 reduction: Effect of ultrasound irradiation, precursor concentration and calcination temperature

Hilmar Guzmán [a,b], Daniela Roldán [a], Nunzio Russo [a], Simelys Hernández [a,b,*]

[a] CREST group, Department of Applied Science and Technology (DISAT), Politecnico di Torino, C.so Duca degli Abruzzi, 24, 10129 Turin, Italy
[b] IIT – Istituto Italiano di Tecnologia, Via Livorno, 60, 10144 Turin, Italy

ARTICLE INFO

Keywords:
Co-precipitation
Ultrasound
Sonochemical synthesis
Copper
Calcination temperature
CO_2 reduction
Electrocatalysts

ABSTRACT

The reduction of high CO_2 concentrations in the atmosphere is an imperative task to reduce the consequences of the greenhouse effect on our planet. Developing active and selective materials for electrochemical CO_2 reduction towards value-added products is mandatory to bring this technology to a practical application. This work studied the effect of assisting Cu and Zn oxides co-precipitation with sonochemistry. Different factors were investigated: the ultrasounds (US) amplitude, the effect of US irradiation time during either precipitation or ageing processes, the precursor concentration and calcination temperature. The synthesised catalysts were tested for the electrocatalytic CO_2 reduction reaction in a Rotating Disk Electrode (RDE) system. Faradaic efficiencies >14% towards alcohols were obtained using US-assisted synthesised Cu-based catalysts. Instead, with the US-prepared Cupper-Zinc-based catalysts, the selectivity towards H_2 and C_1 products (CO and formate) was improved, and the syngas productivity was increased by $> \sim$1.4-fold compared to the non-sonicated one. The alcohols production of the best Cu-catalyst was also confirmed on scalable electrodes. Controlling the synthesis conditions allowed to tune the physicochemical properties of the nanoparticles, including specific surface area, porosity, crystallite size and phases. Mesoporous materials with a mean pores size of around 25 nm were found to induce a better CO_2 diffusion and CO retention time in the porous network, improving the *CO intermediate adsorption at active sites, promoting its dimerisation and thus enhancing the selectivity towards C_{2+} alcohols. The here reported results open the way for new electrocatalysts designs with properly tuned porosity for the selective CO_2 conversion to different valuable products.

1. Introduction

Carbon dioxide is a greenhouse gas found as a trace in the atmosphere. Despite this, it has been declared as one of the major drivers of the greenhouse effect. Its tendency over time has increased since the industrial revolution; this behaviour is mainly attributed to sources from human action. Nevertheless, in 2020 an unusual event occurred with respect to this gas, there was a decrease in global energy-related carbon emissions; these fell by 5.8%, that is, about 2 gigatons of carbon dioxide, thanks to the reduction in the demand for oil, coal, and gas, according to a report by the International Energy Agency (IEA) [1]. However, this reduction does not have a significant long-term impact on global temperatures as they depend on cumulative emissions in the atmosphere. In fact, this unusual event represented just an oasis in the middle of the desert.

Increasing CO_2 in the atmosphere continues and is becoming more and more pressing. In this context, alternatives that reduce greenhouse gas emissions and increase energy supply are especially attractive. One of these alternatives is electrochemical CO_2 reduction (EC CO_2R). The EC CO_2R is especially attractive due to its potential application in storing CO_2 in high-energy products [2,3]. Among the different reduction products, CO is one of the sustainable and simplest products [4]. Indeed, CO formation follows the simplest electrocatalytic CO_2 reduction reaction with 2 e^- transfer. Thus, it is the most studied product in the literature. For this purpose, noble metals such as Ag have been deeply investigated because of their excellent performance. Nonetheless, to

* Corresponding author at: CREST group, Department of Applied Science and Technology (DISAT), Politecnico di Torino, C.so Duca degli Abruzzi, 24, 10129 Turin, Italy.
E-mail address: simelys.hernandez@polito.it (S. Hernández).

https://doi.org/10.1016/j.susmat.2022.e00557
Received 19 February 2022; Received in revised form 16 July 2022; Accepted 14 December 2022
Available online 16 December 2022

overcome obstacles such as the high cost of those materials, earth-abundant and inexpensive metals, including Cu, Zn, and Cd, have been explored and investigated for the electrochemical production of CO from CO_2 [5,6]. Conversely, liquid products (C_{1+}) from CO_2 could lead to a faster transition towards a low C-based economy since they can be stored under ambient conditions. In this regard, methanol and other alcohols (>C_2), like ethanol, are of particular interest [7,8]. These compounds are usually favoured using copper-based electrocatalyst with different structures (Cu nanoparticles, oxide-derived Cu, and Cu composites). Although, other types of materials have been found (e.g. FeP nanoarray on Ti mesh) that have achieved good efficiencies for highly selective EC CO_2R to alcohols [9,10].

Regarding the relevance of using copper-based catalysts for EC CO_2R, a previous review work of our group [11] mentions the most recent advances in the electrochemical transformation of CO_2 towards alcohols by using copper-based catalysts. The study confirmed how different authors have used copper-based catalysts to valorise CO_2 with successful results in several cases. As shown in the review, the catalysts performance depends on different factors such as the electrolyte, catalyst morphology, composition, and cell configuration, among others. Copper has also been combined with different amphoteric metal oxides like ZnO to improve its performance. ZnO has been used as a support to obtain a better distribution of the active catalytic sites, which in some cases means a greater selectivity towards products of interest such as alcohols [12]. Another advantage of Zn in terms of the available active surface area is that it prevents the poisoning and deactivation of copper [13]. It makes the interaction between Cu and Zn oxides in the same catalytic material an interesting object of study.

In this context, many types of synthesis have been investigated to prepare copper-based catalysts, including co-precipitation, sol-gel, hydrothermal, thermal decomposition, microwave irradiation, thermal and sonochemical processes [14]. Each one with its advantages and disadvantages according to each context. The co-precipitation technique is probably the simplest and most efficient chemical pathway through which many nanoparticles can be synthesised. Moreover, it is an environment-friendly and economical method [15]. This method provides homogeneity control through various synthesis parameters (concentration, temperature, pH). Hence, this work used the co-precipitation technique to synthesise Cu-based catalysts. In addition, it was decided to use sonochemistry to study the effect that it would have on the physicochemical characteristics of the catalysts and their selectivity in the EC CO_2R.

Sonochemistry involves wave motion to generate chemical reactions due to the physical phenomena produced by ultrasounds (US). The significant advantage of the sonochemical synthesis approach is the cost-effectiveness, high reaction rate, controllable synthesis condition, narrow size distribution, environmentally friendly nature and scalability [16]. The main physical phenomenon involved in sonochemistry is acoustic cavitation. Acoustic cavitation consists of the formation, growth, and collapse of bubbles in a solution [17]. Consequently, high temperatures and high pressures are observed for very short lifetimes; these transient and localised hot spots facilitate chemical reactions during synthesis [18].

Crystallisation is one of the aspects influenced by US irradiation. According to Luque de Castro and Priego-Capote [19], an effect of ultrasounds on nucleation is shortening the induction time between the establishment of supersaturation and the onset of nucleation and crystallisation. These authors also state that applying ultrasounds induces nucleation and increases reproducibility. In addition, a beneficial effect on the prevention of agglomeration has also been described since the conditions generated after the implosion of cavitation bubbles cause the contact between particles to be shorter than usual and decrease the interaction that holds them together.

Regarding the synthesis of Cu-based catalysts through this technique for thermocatalytic applications, Allahyari et al. [20] synthesised a catalyst called CuO-ZnO-Al_2O_3/HZSM-5 (CZAZ) by ultrasound-assisted co-precipitation method at different irradiation times, which was characterised and tested for the direct synthesis of dimethyl ether from syngas at high temperatures and pressures. They observed a synergetic effect between the ultrasounds and the precipitation that provides a favourable environment for the nucleation and growth of the particles. They also observed that as the ultrasound irradiation time increases, the CZAZ nanoaggregates become smaller, with a low tendency to agglomerate. In another work by Yap et al. [21], the effect of the use of ultrasound in co-precipitation for the synthesis of copper-manganese oxide catalysts was evaluated. The US synthesised catalyst increased methane conversions with respect to the non-sonicated material. They observed alterations in the morphology of the materials, better dispersion of the particles, an increase in the surface area, and were able to tune the conversion rate by varying the intensity of the applied radiation. Dasireddy and Likozar [22] explored the different synthetic methods for the Cu/Zn/Al catalyst: co-precipitation, ultrasonic, sol-gel and solid-state methods for CO_2 hydrogenation to methanol. They observed that the preparation method significantly influences the physicochemical properties and the catalytic performance. They also concluded that among the preparation techniques that they studied, the ultrasonic method improved the dispersion of copper particles, increased the number of active sites, and reached significant selectivity values towards methanol compared to conventional synthetic techniques.

Ultrasounds have also been employed to prepare different metal oxides with other wet synthesis techniques for different applications. For instance, Pinjari et al. [23] synthesised nanostructured titanium dioxide by using conventional and ultrasound-assisted sol-gel techniques to understand the role of cavitation effects in the synthesis process. They found that synthesis in the presence of ultrasounds resulted in a much higher yield, and this is attributed to the ability of acoustic cavitation to improve reaction kinetics through improved mass transfer. They also stated that the development of ordered surface morphology is a characteristic of the US process.

Theoretical concepts and results, such as those previously mentioned, motivated the interest in using ultrasound-assisted co-precipitation to synthesise new catalysts to be exploited in the emerging field of the electrocatalytic conversion of CO_2. In this work, Cu and Cu—Zn— based catalysts were synthesised by this method and tested for the EC CO_2R process. To the best of our knowledge there are no other published works in which sonochemistry and precipitation are jointly used to obtain copper-based materials for the electrochemical reduction of CO_2. Instead, there are works in which sonoelectrochemistry has been used with Cu-based electrodes to improve the CO_2 reduction process, such as those of Ohta et al. [24] and Islam et al [25]. However, their approach is completely different since ultrasounds are applied directly to the electrochemical reactor during the electroreduction process.

Herein, we applied for the first time the sonochemistry technique in the development of catalysts for the EC CO_2R and analysed the different factors that could influence the material performance. Thus, a comparison was made between catalysts synthesised without the US and assisted by US irradiation. Regarding the US-assisted synthesis, the effect of different irradiation times during the precipitation process and amplitudes of ultrasonic power were studied. On the other hand, the influence of the increase in the precursor concentration was also studied, together with the use of US, to evaluate if there was any synergy between these factors that affected both the physical results and the performance of the catalysts. In addition, the effect of calcination temperature (between 250 °C and 550 °C) on the best-performing catalysts was investigated to evaluate the effect of the particle size and the porosity of the material on its electrocatalytic performance [26]. In fact, the porosity can affect the mass transport of the reagents and reaction intermediates [27]. It could influence the retention time and interaction between CO* intermediates (Selectivity Determining Step), which would lead to an increase in selectivity towards products with two or more carbon atoms [11]. Finally, with these variations in the synthesis

process, the aim is to understand better the parameters that can influence the performance of a catalyst and the techniques that can be used to tune the optimal physicochemical characteristics for the CO_2 electroreduction process.

2. Materials and methods

2.1. Materials

Copper (II) nitrate trihydrate ($CuN_2O_6{\cdot}3H_2O$, 99–104 %). Zinc nitrate hexahydrate crystallised ($Zn(NO_3)_2{\cdot}6H_2O$, ≥99.0 %). Potassium bicarbonate ($KHCO_3$, 99.7%). Nafion perfluorinated resin solution Green Alternative (5 wt% in lower aliphatic alcohols and water contains 15–20 % water). Sodium Carbonate (Na_2CO_3, ≥99 %). Isopropanol for HPLC ($(CH_3)_2CHOH$, 99%). All the materials were purchased from Sigma-Aldrich and used as received unless otherwise specified.

2.2. Synthesis

The catalysts were prepared with a procedure analogous to that proposed by Schüth et al. [28]. Herein, different variations were made to evaluate the effect of some parameters on the synthesis (i.e., ultrasound amplitude applied during the ageing time, Cu concentration, ultrasound irradiation time during the precipitation, calcination temperature). Amphoteric metal oxides like ZnO are traditionally investigated as metal supports of Cu materials for the CO_2 hydrogenation to CO and methanol at high temperature and pressure. However, we have recently demonstrated that a Cu/ZnO (65/35%mol) catalyst prepared by the low-temperature oxidation of Cu nanoparticles and its mixing with ZnO crystalline powder can be used for the electrochemical CO_2 reduction to alcohols [12]. The presence of ZnO nanoparticles with this composition (65 %mol) in the mixed Cu/ZnO catalyst was found to play an important role in forming and stabilising mixed oxidation states of copper (Cu^{1+} and Cu^0) in the electrocatalyst (in bulk and surface). Based on those results, it was chosen as the precursor ratio for preparing the mixed metal oxide. On the other hand, we also have proved that a copper oxide catalyst synthesised with a copper nitrate concentration of 0.6 M has high selectivity towards the formation of hydrocarbons and multicarbon oxygenates (including aldehydes and alcohols) [29]. Thus, it was the selected concentration for synthesising the bare copper material and studying the abovementioned effects.

Regarding the synthesis process, the metal nitrates used for each catalyst and their concentration are reported in Table 1. A sodium carbonate solution (1 M) was used as the precipitating agent. The setup consists of a beaker with a volume of 200 mL of distilled water immersed in a hot silicone oil bath to maintain the temperature at 70 °C. The temperature was monitored with a thermocouple. The pH was controlled by an MC720 pH Controller, which regulated the amount of precipitating agent sent to the beaker to maintain a constant pH value of 7.

The setup of the synthesis is shown in Fig. 1. It consists of two peristaltic pumps, one that is part of the pH controller and regulates the flow rate of precipitating agent and another that regulates the nitrate solution flow rate.

After adding the 40 mL of the nitrate precursor, the system was left ageing for one hour; then, the precipitate was filtered and left drying overnight at 60 °C in an oven. Finally, the calcination was carried out with 500 mg of catalyst in a furnace for 3 h at a certain temperature with a heating ramp of 2 °C min^{-1}.

The ultrasound effect was evaluated during the co-precipitation time and in the ageing time using an Ultrasonic Processors VCX 750 (Frequency: 20 kHz, Net power output: 750 W). The sonicator has amplitude settings. It tells how vigorously the particles vibrate, which is proportional to the square root of intensity. The amplitude/intensity is proportional to the operating voltage; thus, the sonication will occur more vigorously as you increase it. The solution was irradiated with different amplitudes of 23 %, 30 %, and 37 % to study the effect on the particle size of the synthesised powders. That and other variations made in the ultrasound-assisted synthesis, such as changes in precursor concentrations, co-precipitation time, and the calcination temperature of the precipitated particles, are shown in Table 1.

% after the name of the resulting calcined catalysts was referred to as the amplitude percentage used for the ultrasound-assisted co-precipitation. A and #P after the applied amplitude percentage (% X) stand for the US conditions: A indicates that the US irradiation was only applied during the ageing process, and P means that the US was used during the co-precipitation time; # is the corresponding precipitation time (i.e. 4, 8, or 12 min). For the latter, the volume of 40 mL of the precursor was kept constant, and its flow rate was 10, 5 and 3.33 mL min^{-1}, respectively. The co-precipitation time was set at 8 min to evaluate the effect of ultrasounds during the ageing process. On the other hand, the calcination was performed at 350 °C in most cases, but when it was changed, the new settled temperature was indicated at the end of the catalyst name (i.e. 250, 450 or 550 °C).

Table 1
Composition of the US-prepared CuZn oxide-based catalysts.

Catalyst	Precursor concentration, M		Amplitude (X), %
	Cu $(NO_3)_2.3H_2O$	Zn $(NO_3)_2.6H_2O$	
CuZ-065-035-(%X)-A-T	0.65	0.35	23 30 37
Cu-06-(%X)-A-T	0.6	–	23 30 37
Cu-06-(%X)-#P-T	0.6	–	30
Cu-1-(%X)-#P-T	1.0	–	30

2.3. Characterisation of powder catalysts

Morphological characterisation and semi-quantitative elemental composition of the samples were obtained by using a ZEISS MERLIN field-emission electron microscope (FE-SEM), equipped with an Energy Dispersive X-ray Spectroscopy System (EDS) that was operated at 3 kV.

The main textural parameters such as the specific surface area, total pore volume and pore size distribution were characterised through N_2 adsorption using a volumetric equipment TriStar II 3020 supplied by Micromeritics. The samples were subjected to a pre-treatment process for 2 h at a temperature of 200 °C to eliminate impurities and humidity. The Brunauer–Emmett–Teller (BET) equation was used to calculate the surface area, and the method of Barrett, Joyner, and Halenda (BJH) was used to calculate the pore size distributions from experimental isotherms by using the Kelvin model of pore filling.

X-Ray Diffraction (XRD) technique was used to obtain information about the crystallinity of the samples by using a Panalytical X'Pert PRO diffractometer working in Bragg-Brentano configuration and equipped with Cu Kα radiation (λ =1.5418 Å) set at 40 kV and 40 mA. Crystallite sizes were calculated by using the Scherrer formula $D = k\lambda / \beta \cos \theta$, where D is the average crystallite size (nm), λ is the wavelength of X-ray radiation (0.15418 nm), k is the shape factor (0.90) and β is the full-width half-maximum.

2.4. Electrochemical cell and experimental conditions

2.4.1. RDE system

The electrochemical activity was evaluated at room temperature and atmospheric pressure using a traditional three-electrodes electrochemical cell. The US-prepared catalysts were deposited on a glassy carbon Rotating Disk Electrode (RDE), which was used as a working electrode (electrode area of 0.1963 cm^2) to eliminate the effects of mass transfer limitations. The counter electrode was a platinum wire, and the

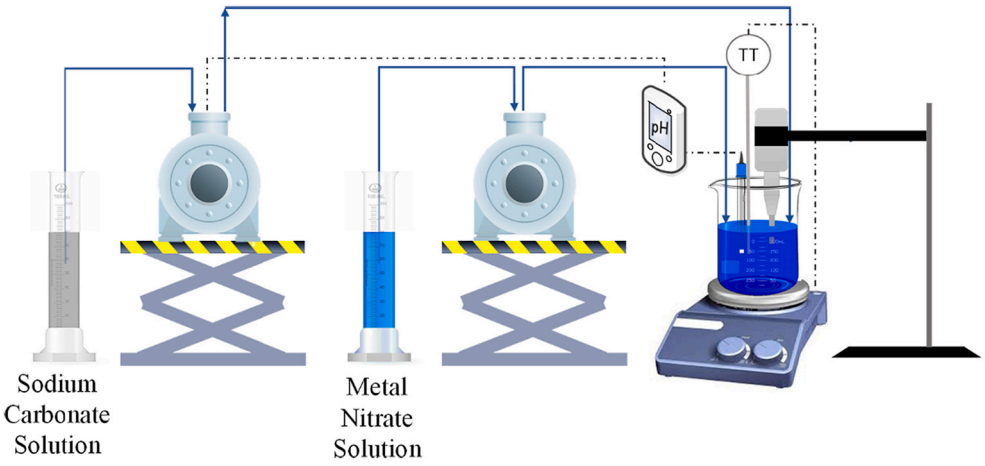

Fig. 1. Synthesis process set up.

reference electrode was a silver/silver chloride electrode (Ag/AgCl, 3 M NaCl). 20 mL of $KHCO_3$ (0.1 M) in water was used as the electrolyte. A Biologic VSP-300 multichannel potentiostat and an RRDE-3A rotator system were used to perform the electrochemical tests. The experimental setup to perform the electrochemical CO_2 reduction has been described in our previous study [29].

The ink was prepared using a Nafion solution as a binder, isopropanol as the carrier, and a percentage of Vulcan XC 72R Carbon (VC, 9.5 wt% of active phase) was added to increase the conductivity of the mixture. The mixture was sonicated for 10 min to obtain a better dispersion of the particles. For the ink preparation, the following ratios were considered: a mass ratio of active phase/Nafion of 70:30 and an isopropanol/solids mass ratio of 97:3.

With a catalyst loading of 0.6 mg_{CuO} cm^{-2}, the electrochemical behaviour was studied using a protocol in N_2 and CO_2 that includes Cyclic Voltammetry (CV), Linear sweep voltammetry (LSV) and Chronoamperometry (CA). Specifically, CV from 0 to -2 V vs Ag/AgCl at a scan rate of 30 mV s^{-1}, LSV from 0 to −3 V vs Ag/AgCl at a scan rate of 5 mV s^{-1} and the electrochemical reduction of CO_2 employing a CA for 2 h under CO_2-saturated electrolyte to evaluate the selectivity of the catalyst. The tests were performed for each catalyst at −0.99 V vs RHE of applied potential after performing a pre-reduction in N_2-saturated 0.1 M $KHCO_3$ aqueous solutions at −0.8 V vs RHE.

The CO_2 flow rate was set via a mass flow controller (EL-Flow Select, PN64) at 8.86 NmL min^{-1}. All the electrochemical measurements were made at a rotation speed of 3700 rpm. The gaseous products were analysed online with a gas chromatograph (Inficon, Micro GC Fusion Gas Analyzer). In contrast, the liquid ones in the electrolyte solution were analysed with a high-performance liquid chromatograph (Shimadzu HPLC, Prominence model with detector RID-10A, SPD-M20A, ELSD-LT II and RF-20A) and with a Perkin Elmer Gas Chromatograph (model Clarus 580) equipped with a Head Space (Turbomatrix 16) and a Stabilwax-DA column.

Thanks to the analysis of liquids and gases just mentioned, it is possible to measure the selectivity of the process towards a specific product utilising the Faradaic efficiency with the following formula:

$$FE\ (\%) = \frac{z \bullet \dot{n} \bullet F}{j \bullet A \bullet t} \bullet 100 \quad (1)$$

Where z is the number of electrons needed for CO_2 reduction, F is the Faraday constant, $\dot{n}$ is the outlet molar flow rate of each product, j is the current density, t is the reaction time, and A is the electrode area.

2.4.2. Electrodes by airbrushing

In addition to the tests carried out using the glassy carbon surface of the RDE as the working electrode, it was decided to carry out additional tests using electrodes supported on carbon paper. It was done for two of the most promising catalysts previously tested in the RDE system. The electrodes were prepared by depositing the catalytic ink on a porous carbon support (Toray carbon paper, TP-060T Quintech) by airbrushing. The catalytic ink was prepared with the same components mentioned in section 2.4.1. The electrodes had a geometric area of 1 cm^2 and a catalyst loading of 1.2 mg_{CuO} cm^{-2}. As for the RDE test, the same cell, electrolyte, counter electrode and reference electrode were used.

On the other hand, the electrochemical behaviour of the catalysts was evaluated at the same CV and LSV conditions. Finally, the electrochemical reduction of CO_2 was carried out employing a chronopotentiometry (CP) at the current density obtained in the chronoamperometry previously carried out in the test performed with the RDE configuration. The system was stirred with a stir bar to avoid mass transfer limitation problems during the test.

3. Results and discussions

3.1. Physico-chemical characterisation of synthesised powder catalysts

3.1.1. Effect of different US amplitudes

The FESEM micrographs of the CuZ-065-035 synthesised catalysts are shown in Fig. 2. Fig. 2(b), (c), and (d) indicate FESEM micrographs of the CuZn catalysts synthesised under different amplitudes. The micrograph of the original CuZ-065-035 was added to compare the differences. The biggest difference between these samples is in the particle agglomeration. Indeed, the samples synthesised with the ultrasound-assisted co-precipitation method show more dispersed, smaller, and more uniform particles than the original precipitated sample CuZ-065-035. It seems that assisting the co-precipitation synthesis with the US offers a uniform environment for the nucleation and growth of the particles while avoiding their agglomeration, similar to the synergistic effect of the ultrasounds observed by Allahyari S. et al. [30]. Smaller particles were obtained at the highest applied amplitudes, probably due to high nucleation rates achieved during these US-assisted precipitations. Instead, the applied amplitude of 23 % was not enough to disaggregate the formed nuclei. Hence, the produced particles are bigger because of a higher agglomeration of the smaller crystallites, as shown in Fig. 2(b).

Contrarily, Fig. 3 shows that the Cu-06 samples synthesised with the US-assisted ageing process do not show different morphologies at different applied amplitudes (23 % and 30 %) compared to the original Cu-06 sample. Instead, as the amplitude increases to 37 %, the porous spherical hierarchical microstructure is incomplete. It seems that the employed applied amplitudes are not enough to obtain more dispersed and smaller particles when only copper nitrate is used as a precursor. It

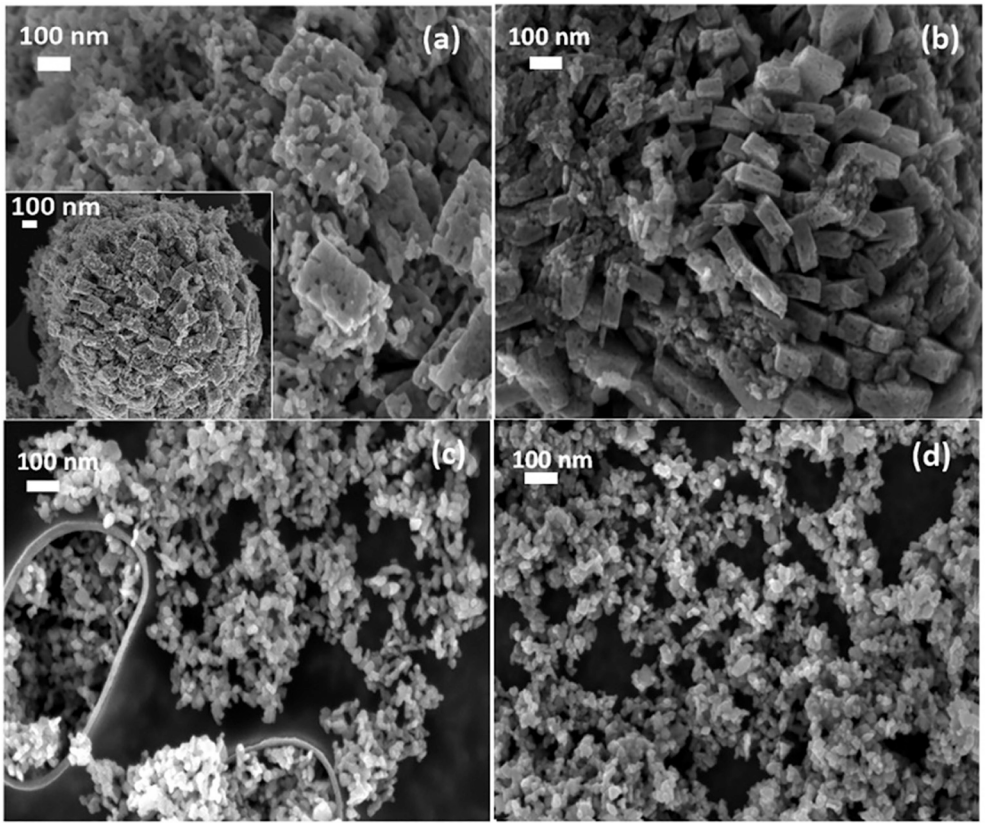

Fig. 2. FESEM micrographs of US-prepared CuZn-oxide based catalysts (a) original CuZ-065-035, (b) CuZ-065-035-%23-A, (c) CuZ-065-035-%30-A and (d) CuZ-065-035-%37-A.

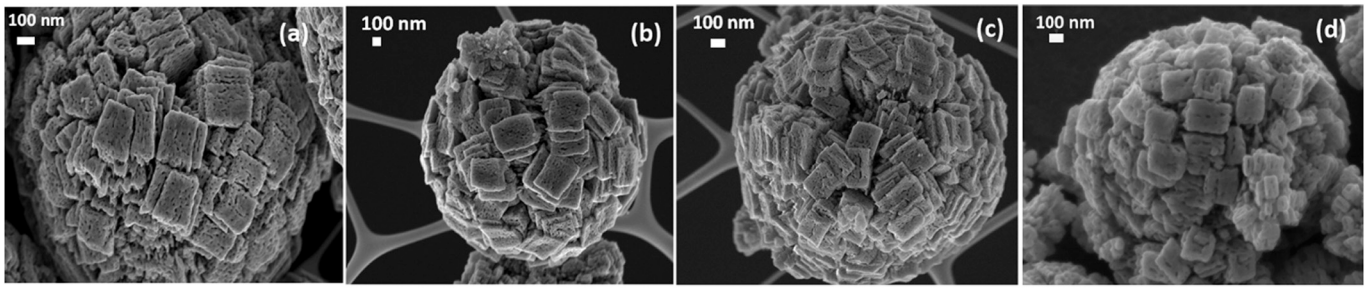

Fig. 3. FESEM micrographs of US-prepared CuO catalysts (a) original Cu-06, (b) Cu-06-%23-A, (c) Cu-06-%30-A, and (d) Cu-06-%37-A.

could demonstrate the role of zinc in increasing the dispersion of copper particles. The textural features of the US-prepared samples were changed concerning the original catalyst. The BET specific surface area, porosity and crystallite size of the samples obtained by irradiating the solution with different US amplitudes are shown in Table 2. The hypothesis is that in the ageing process, the stability of the developed crystalline phases differs depending on the amplitude used. These precipitates are constituted by mixtures of metal-hydroxy-carbonate phases, which decompose during the calcination treatment to produce well-dispersed oxidic phases. The decomposition of these different stable phases gives place to a different porosity in the structure.

The use of ultrasound has increased the specific surface area of the CuZ-065-035 sonicated sample at.% 23 of amplitude compared to the non-sonicated one, which agrees with the literature [18]. The higher BET surface area of the %23 sample is probably due to the smaller crystallites of ZnO (CuO crystals are similar among all the samples). Instead, the specific surface area decreased by increasing the applied US amplitude. In agreement with this, the total pore volume decreased at the highest amplitude percentage (% 37), as demonstrated by the results of nitrogen uptake measurements (see Table 2) and the pore size of the catalysts that became wider by increasing the US amplitude, see Fig. 4 (a). Moreover, a higher ZnO crystals size and an improved crystallinity were observed at the highest applied amplitudes. In this regard, a higher exposure of the CuO (111) and new facets of CuO (202) and ZnO (002) and (103) are evident from the XRD spectra in Fig. 5(c) and (d). The effect of acoustic cavitation generates a transient high temperature, pressure and strong stirring power that benefit smaller and more porous nanoparticles [31,32]. In this regard, the CuZ-065-035 presents a bimodal pore size distribution, showing peaks centred at 10 and 30 nm, while the US-prepared catalyst shows a dominating diameter of 30 nm. The BJH pore size distribution plots confirm the disordered mesopores structures.

Unlike the CuZn catalysts, the bare CuO materials do not show appreciable differences in the crystalline structure. In fact, there are no changes between the original and the new US-prepared Cu-06 catalysts (see Fig. S1). However, the BET surface area at 23 % and 30 % of US

Table 2
Main textural parameters of the US-assisted CuZn oxide-based catalysts.

Catalyst	BET surface area, $m^2 g^{-1}$	ECSA, $cm^2 g^-$	Total pore volume, $cm^3 g^{-1}$	EDS, atomic ratio	Crystallite size, nm	
					(11−1) facet of CuO	(100) facet of ZnO
CuZ-065-035	54.64	3.02	0.19	Cu/Zn 63:37	6	7
CuZ-065-035-%23-A	60.68	3.43	0.23	Cu/Zn 57:43	7	6
CuZ-065-035-%30-A	50.81	4.37	0.25	Cu/Zn 58:41	7	12
CuZ-065-035-%37-A	26.11	4.50	0.07	Cu/Zn 60:40	7	10
Cu-06	18.40	2.40	0.11	Cu/O 1:1	17	–
Cu-06-%23-A	34.07	2.77	0.14	Cu/O 1:1	14	–
Cu-06-%30-A	32.07	1.66	0.13	Cu/O 1:1	14	–
Cu-06-%37-A	18.68	3.53	0.12	Cu/O 1:1	16	–

amplitude increased by ~100 % with respect to the original sample (Table 2). In agreement with this, the pores size distribution shift to smaller values with and slightly smaller CuO crystallites, corresponding to the (11–1) facet, were produced by assisting the co-precipitation synthesis with these US intensities (see Table 2). For the Cu-06-%37-A, a decrease in BET surface area was observed, probably due to the larger crystallite size obtained. This amplitude value appears to be a critical value for which the crystallite and pore size are similar to the original material (see Table 2 and Fig. 4(b)).

3.1.2. *Effect of different Cu concentration*

A catalyst with a more concentrated Cu nitrate solution (1 M) was synthesised to compare the influence of the precursor concentration on the textural features. The synthesis was assisted with the US during the ageing process at 30 % of amplitude. As shown in Fig. 6, increasing the Cu precursor concentration to 1 M (Cu-1-%30-A) influences the morphology of the formed porous spherical hierarchical microstructures vs. the Cu-06-%30-A. As the copper nitrate precursor concentration increases, CuO formation is incomplete at the investigated ageing time. Nevertheless, the CuO structure grew from a common nucleation point in both cases.

It is worth mentioning that increasing the copper nitrate concentration resulted in the formation of slightly larger CuO crystallite sizes (from 14 to 15 nm), corresponding to the (11–1) facet, as shown in Table 3. It can be attributed to a synergetic effect of the presence of the US and the higher supersaturation. Moreover, larger pores were obtained by increasing the precursor concentration (Fig. 7(a)), in agreement with the decrease of 18% of the BET surface area (see Table 3).

3.1.3. *Effect of different precipitation times*

Fig. 8 illustrates the FESEM micrographs obtained by varying the precipitation time in the US-assisted synthesis. Particles with spherical shapes were obtained with the previously used precipitation time of 8 min, as shown in Fig. 8(b). When the time decrease to 4 min or increase to 12 min, the spherical morphology is not fully formed (Fig. 8 (a) and (c)). However, the particles grow from a common nucleation point in all cases.

The variations made during the US-assisted synthesis of the Cu-06 catalyst produce a modification in the spherical hierarchical original structure. However, the inter-particle collisions during sonication do not significantly influence the size of these big particles. Although ultrasound is a method to obtain more dispersed, de-agglomerate and smaller nanoparticles in aqueous media, it probably requires high specific energy inputs to overcome the adhesive forces in the case of the CuO synthesis process. Nevertheless, the US-assisted precipitation for 8 min reached an optimum with a higher specific surface area (~ 32 $m^2 g^{-1}$) than the 4 and 12 min precipitation time (see Table 3). Regarding the pores size distribution, there are no significant differences between the samples precipitated for 4 and 8 min. However, the increase of the US-assisted precipitation time to 12 min leads to the formation of bigger pores (see Fig. 7(b)).

3.1.4. *Effect of calcination temperature*

The changes in the calcination temperature were evaluated for the powders produced by US-assisted co-precipitation synthesis for 8 min. Morphological differences are observed. Although spherical structures are observed in all cases, the external rectangular structures are of different sizes, indicating the sintering of the crystallites by increasing the calcination temperature (see Fig. S2). It probably produces changes in porosity. In fact, Table 3 shows that the obtained specific surface area increased of 1.9-fold by decreasing the calcination temperature to 250 °C (with respect to the previously used: 350 °C for the Cu-06-%30-8P sample). The pore size distribution is narrower and smaller by decreasing the calcination temperature, as shown in Fig. 7(c). Contrarily, the total pore volume and specific surface area decreased by increasing the calcination temperature, probably due to the increase of the particles size and degree of agglomeration by the effect of sintering

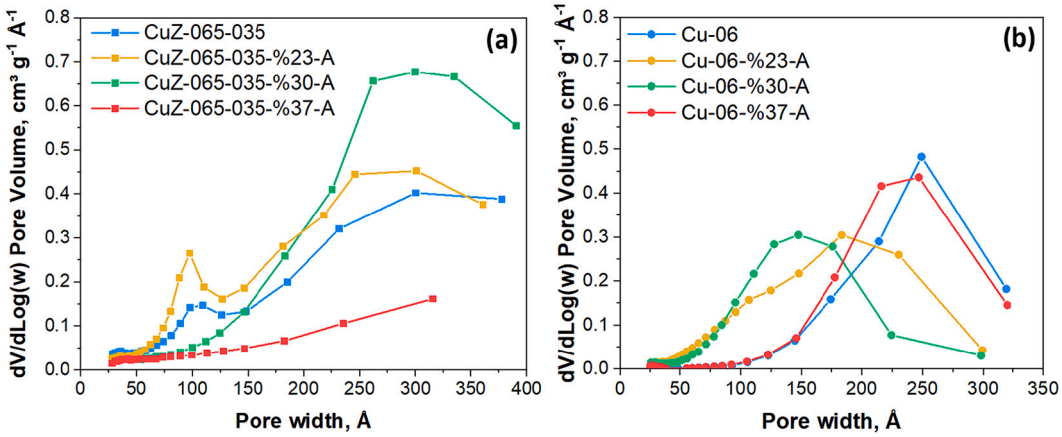

Fig. 4. BJH pore size distribution curves of the US-prepared CuZnoxide-based samples: (a) CuZ-065-035 and (b) Cu-06.

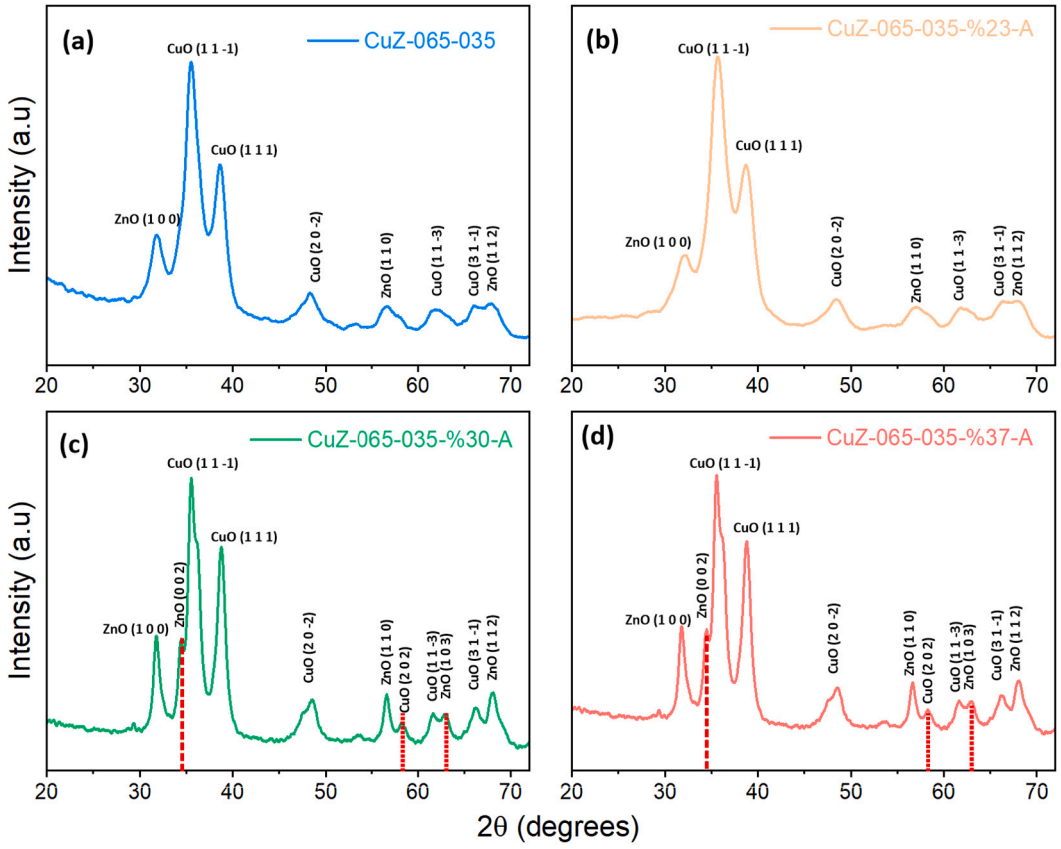

Fig. 5. XRD patterns of US-prepared CuZn-oxide based catalysts (a) original CuZ-065-035, (b) CuZ-065-035-%23-A, (c) CuZ-065-035-%30-A, and (d) CuZ-065-035-%37-A.

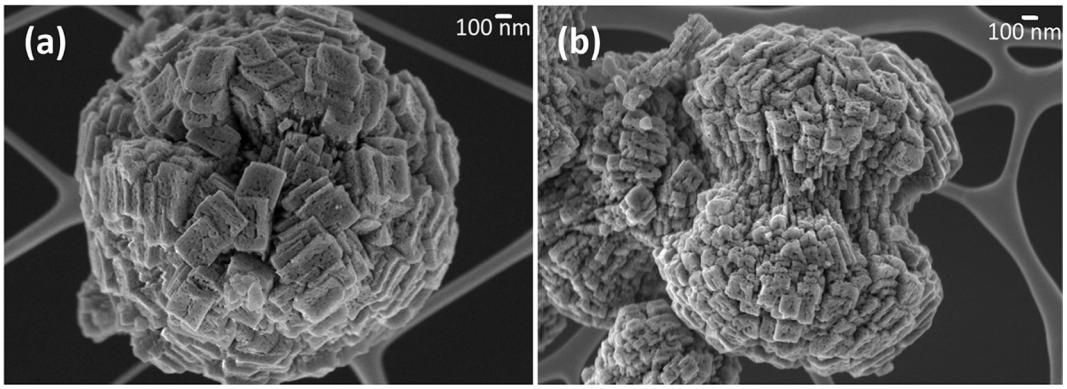

Fig. 6. FESEM micrographs of the effect of precursor concentration in the US-prepared CuO catalysts (a) Cu-06-%30-A and (b) Cu-1-%30-A.

occurred in the material [26].

In addition, the X-ray diffraction peaks can be assigned to the monoclinic CuO crystalline phase and to the same facets found for the original Cu-06 (see Fig. S1). Table 3 demonstrates the low increase of crystallite size in the range of calcination temperatures evaluated (250 °C – 550 °C), most probably due to the presence of water molecules and hydroxy carbonate groups, which prevents the rapid crystals growth.

3.2. Electrochemical measurements

3.2.1. Effect of different US amplitudes on electroactivity for EC CO_2R

The electrocatalytic performance of the CuZ-065-035 and Cu-06 samples prepared without and with the US-assisted co-precipitation (at an applied amplitude of 30 %) was determined for the electrochemical CO_2 reduction reaction in CO_2-saturated 0.1 M $KHCO_3$ solution.

As shown in Fig. 9(a), the US-prepared CuZ catalyst and CuZ-065-035 LSV curves exhibit a similar performance, indicating that the prepared materials have similar electrocatalytic activity for the CO_2 reduction reaction. This behaviour is also evidenced by the time evolution of the current density during the CO_2 co-electrolysis in Fig. 9(b). The current density in both cases increases towards more negative values by about 25 % after 60 min of testing. However, the US-prepared CuZ catalyst reached a slightly higher current density with respect to the original CuZ-065-035. This result correlates well with the increased

Table 3
Main textural parameters of the US-assisted CuO-based catalysts.

Catalyst	BET surface area, $m^2\ g^{-1}$	ECSA, $cm^2\ g^{-}$	Total pore volume, $cm^3\ g^{-1}$	Crystallite size, nm
				(11–1) facet of CuO
Cu-06-%30-A	32.07	1.66	0.13	14
Cu-1-%30-A	26.27	3.72	0.14	15
Cu-06-%30-4P	25.13	4.22	0.12	14
Cu-06-%30-8P	31.55	3.62	0.13	15
Cu-06-%30-12P	20.37	2.58	0.10	15
Cu-06-%30-8P-250 °C	58.64	6.46	0.14	10
Cu-06-%30-8P-450 °C	16.54	3.10	0.08	14
Cu-06-%30-8P-550 °C	10.96	1.28	0.05	14

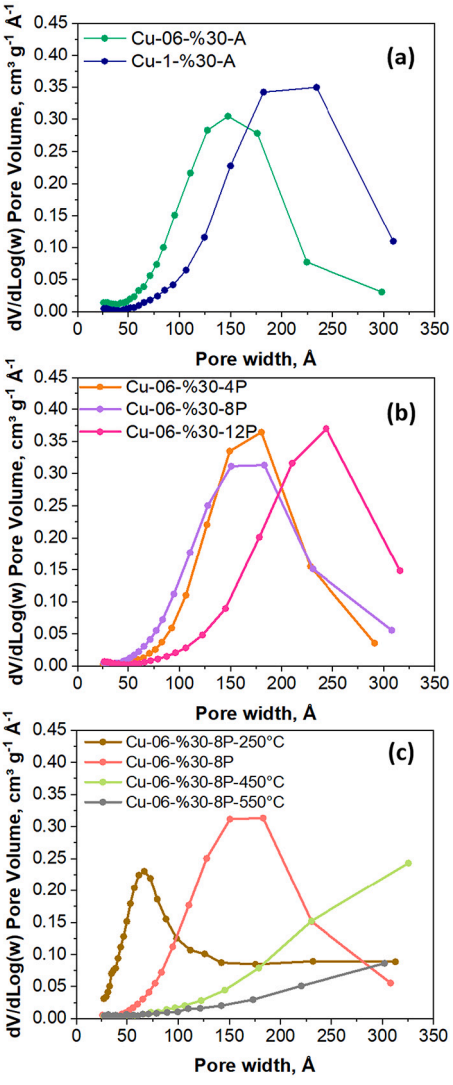

Fig. 7. BJH pore size distribution curves of the US-prepared CuO samples: (a) effect of copper concentration, (b) effect of temperature calcination and (c) effect of precipitation time.

availability of electrochemically active sites showed by the US-catalyst (see ECSA results in Table 2) and agrees with a recently published work demonstrating that the geometric current density (reductive current with respect to the geometric surface area) under CO_2 increases with the roughness of the catalysts [33]. Fig. 9(c) and (d) evidence the various products, including ethanol, acetone, formate, CO, hydrogen, and a little amount of methanol, that were detected.

In detail, the original CuZ-065-035 achieved a total Faradaic efficiency towards C_{2+} products of ~ 11 %, whereas the US-prepared material produced ~ 1.5 % as maximum FE for C_{2+} products at this negative applied potential. It is worth noting that a small quantity of methanol was produced with the CuZ-065-035-%30-A sample. It indicates that the smaller and less agglomerated particles induced from the US-assisted co-precipitation synthesis decrease the selectivity of C_{2+} products. At the same time, the US-prepared CuZ catalyst increased by ~1.4 fold the syngas (H_2/CO) productivity. Based on the previously mentioned physicochemical characteristics of this material, the higher selectivity for syngas of the US-prepared CuZ-based catalyst could be attributed to their smaller particle sizes and higher pore volume structure than the not US-prepared materials [34–39]. In particular, the desorption of the first intermediate *CO is probably favoured, thus reducing its residence time inside the catalyst for its further reduction or/and for C—C bonds formation by *CO dimerisation reactions. In fact, as aforementioned, the original CuZ presents pores smaller than 10 nm that could increase the residence time of these intermediates, promoting the formation of more reduced products.

Additionally, the influence of the thickness of the catalytic layer on the selectivity for CO2 reduction reaction was evaluated. The registered current density increased by increasing the used catalyst loading (Fig. 10 (a)). In all cases, the current profile was not stable with time during the entire period. During the first 10 min, the current density slightly decreased. It could be ascribed to insufficient porosity in the thickness of the catalytic layer, causing the accumulation of gaseous product bubbles and, subsequently, the partial block of catalytic sites. Then, the current densities unquestionably decreased (become more negative). This instability could be attributed to the material reducing from CuO to Cu if the previously applied pre-reduction was insufficient. Interestingly, when 0.2 mg cm-2 was used as the catalyst loading, the FE towards C2+ products was slightly increased to 2% (Fig. 10(b)). However, this catalyst loading decreased the electrocatalytic activity (J) by about 50%.

The results obtained for the original Cu-06 and Cu-06-%30-A are shown in Fig. 11. As revealed by the LSV curves in Fig. 11(a), the US-prepared Cu-06-%30-A achieved a total current density of about −50 mA cm^{-2} at −2.5 V vs RHE, which was lower than that of the original Cu-06 catalyst (−70 mA cm^{-2}). This performance indicates that the latter has a better electrocatalytic activity for the CO_2 reduction reaction. The long-term stability was tested at −0.99 V vs RHE. The US-prepared CuO catalyst displayed the lowest current density, which is in agreement with the roughness factor as in the case of CZ materials. Indeed, the Cu-06-%30-A catalyst has a lower electrochemical active area (ECSA) than the original Cu material. However, it showed better stability during the entire test than the original Cu-06 sample (Fig. 11 (b)). The Faradaic efficiency and productivities of the detected gas and liquid products are exhibited in Fig. 11(c) and (d). The selectivity towards more reduced products is 2-fold lower for the US-prepared catalyst than in the original one. However, methanol was again detected on the US-prepared catalyst. Both materials present spherical hierarchical microstructures formed by porous pyramids (see Fig. 3). The Cu-06-%30-A presents twice the surface area of the original Cu-06 (see Table 2), which is related to the effect of sonication. In addition, ultrasonic irradiation affects the formation of tight porosity, with a dominating diameter of 15 nm in the case of Cu-06-%30-A, while original Cu-06 presents a well-ordered mesopore structure with a pore size of 26 nm (see Fig. 4(b)). The best electrocatalytic activity for the CO_2 reduction reaction could be related to the diffusion properties of as synthesised catalysts. The well-ordered mesopore structure could enhance the

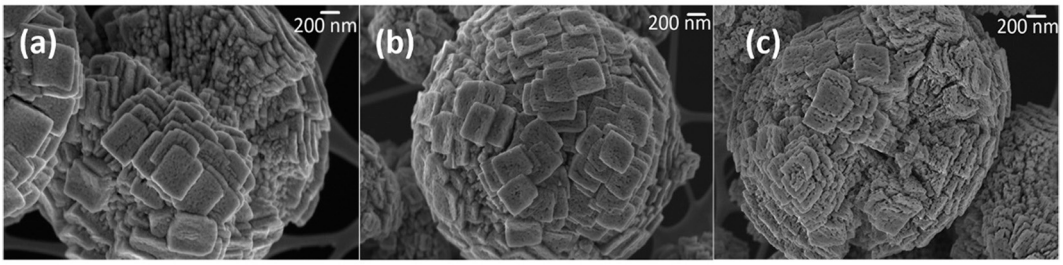

Fig. 8. FESEM micrographs of the effect of co-precipitation time in the US-prepared CuO catalysts (a) Cu-06-%30-4P, (b) Cu-06-%30-8P, and (c) Cu-06-%30-12P.

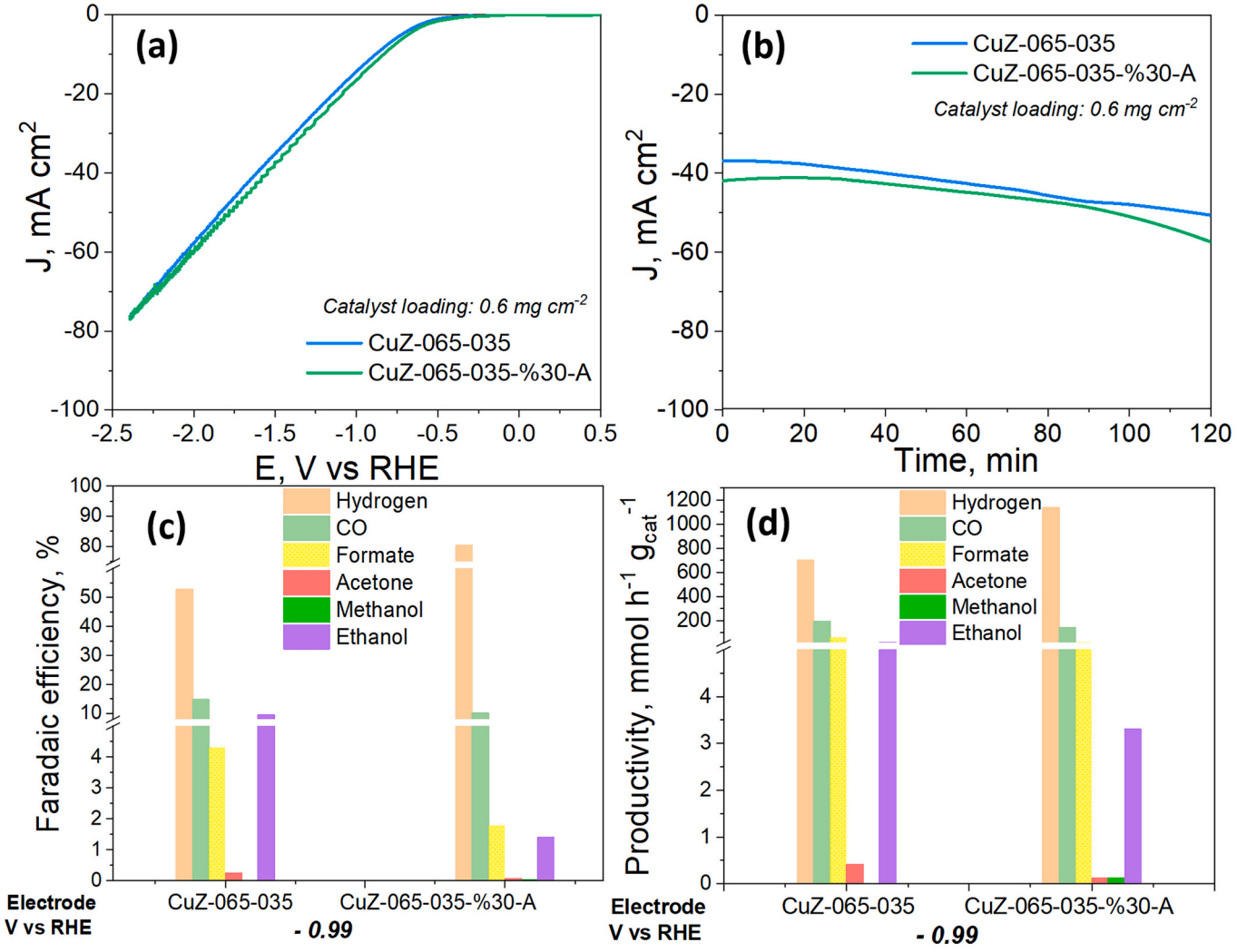

Fig. 9. Linear sweep voltammetry responses (a), evolution time of the total current density of the electrochemical reduction of CO_2 (b), Faradaic efficiencies (c) and productivities of gas and liquid products (d) for CuZ-065-035 and CuZ-065-035-%30-A (0.6 mg cm^{-2}) tested in 1 M $KHCO_3$ aqueous electrolyte at −0.99 V vs RHE.

suitable diffusion, adsorption, and subsequent reduction of reagents and intermediates of the reaction.

The catalyst loading effect was also evaluated for this US-prepared Cu-06 catalyst at 30 % applied amplitude (Fig. 12). As in the previous case, a lower catalyst loading further confirms the higher selectivity for C_{2+} products, while higher catalyst amounts increased the C_1 products like CO and formate, indicating the role of a suitable porosity in the thickness of the catalytic layer on the selectivity of the electrochemical reaction.

Fig. 13 shows the correlation between the Faradaic efficiencies of the products obtained on the different CuZ and Cu catalysts prepared using ultrasonic irradiation at different amplitude percentages and the correlation with the total pore volume. The comparison was carried out with a catalyst loading of 0.2 mg cm^{-2}.

In the case of CuZ, from % 23 to % 37 of applied amplitude, the FE to ethanol is reduced (from ~3 % up to ~0.8 %) in the same way that the catalyst particles become more dispersed (less agglomerated in larger particles), as shown in Fig. 2. Besides, the CuZ-065-035-%23-A material shows the lowest ECSA value although it has the highest BET surface area (see Table 2), suggesting that not the entire surface of the catalyst participates in the electrocatalytic reactions. It could be attributed to the shape and length of the porous channels, which could generate

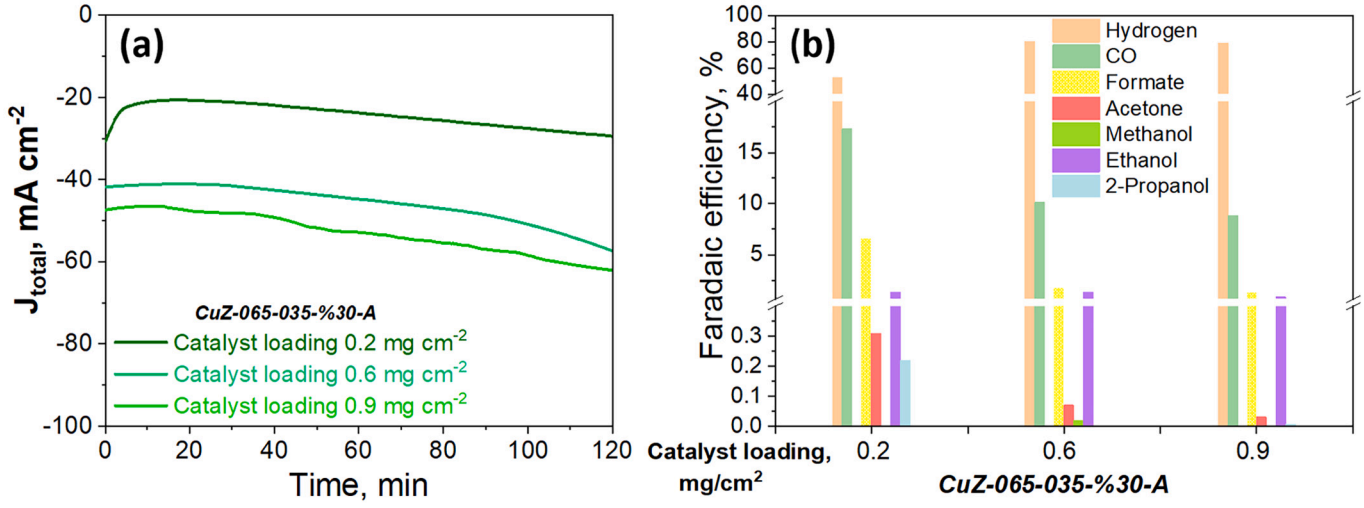

Fig. 10. Chronoamperometry responses (a) and Faradaic efficiencies for CuZ-065-035-%30-A catalyst with different catalyst loading tested in 1 M $KHCO_3$ aqueous electrolyte at −0.99 V vs RHE.

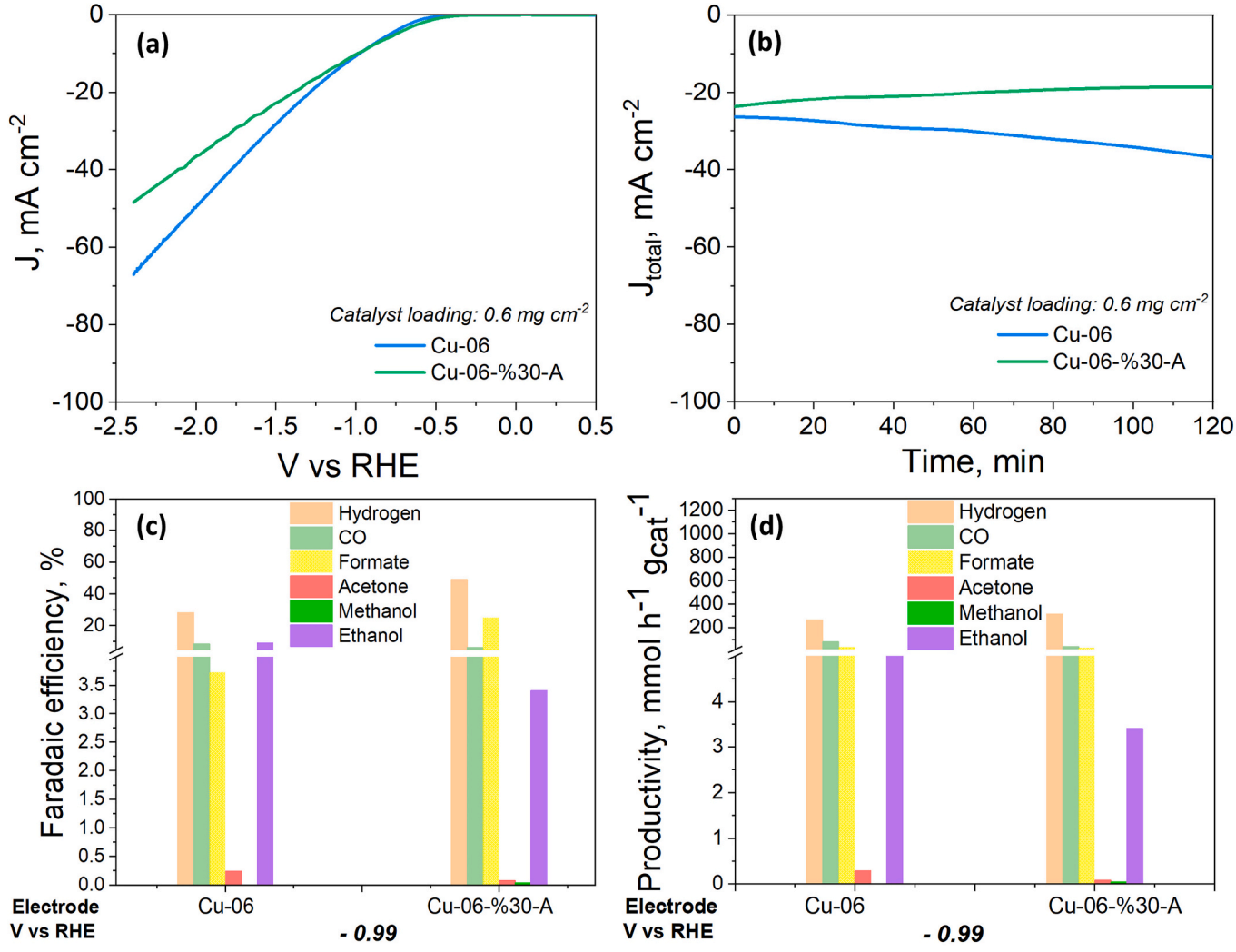

Fig. 11. Linear sweep voltammetry responses (a), evolution time of the total current density of the electrochemical reduction of CO_2 (b), Faradaic efficiencies (c) and productivities of gas and liquid products (e) for Cu-06 and Cu-06-%30-A (0.6 mg cm^{-2}) tested in 1 M $KHCO_3$ aqueous electrolyte at −0.99 V vs RHE.

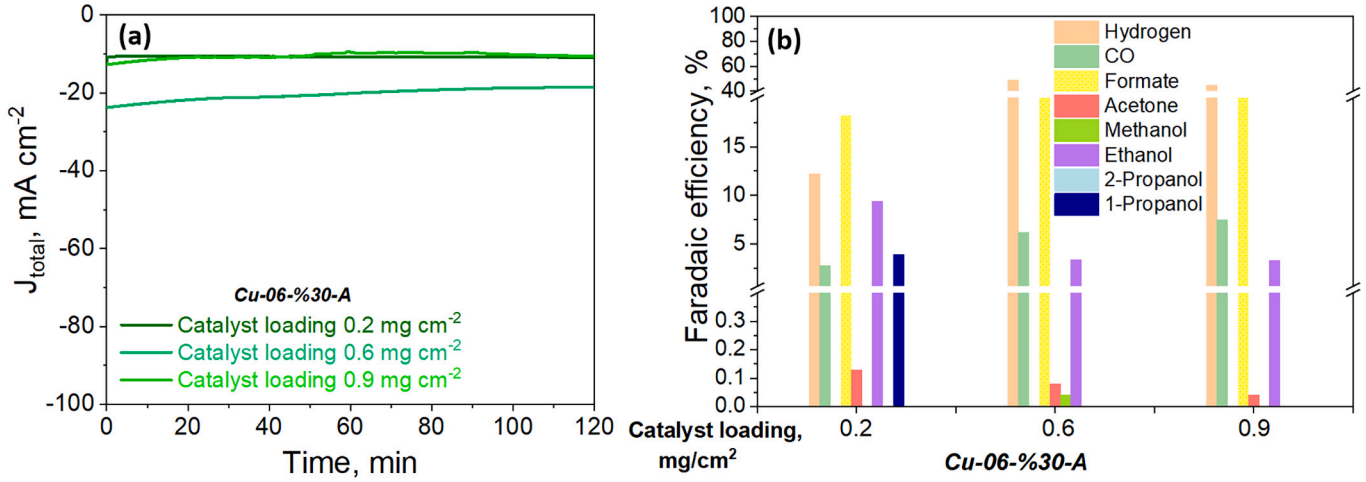

Fig. 12. Chronoamperometry responses (a) and Faradaic efficiencies for Cu-06-%30-A catalyst with different catalyst loading tested in 1 M $KHCO_3$ aqueous electrolyte at −0.99 V vs RHE.

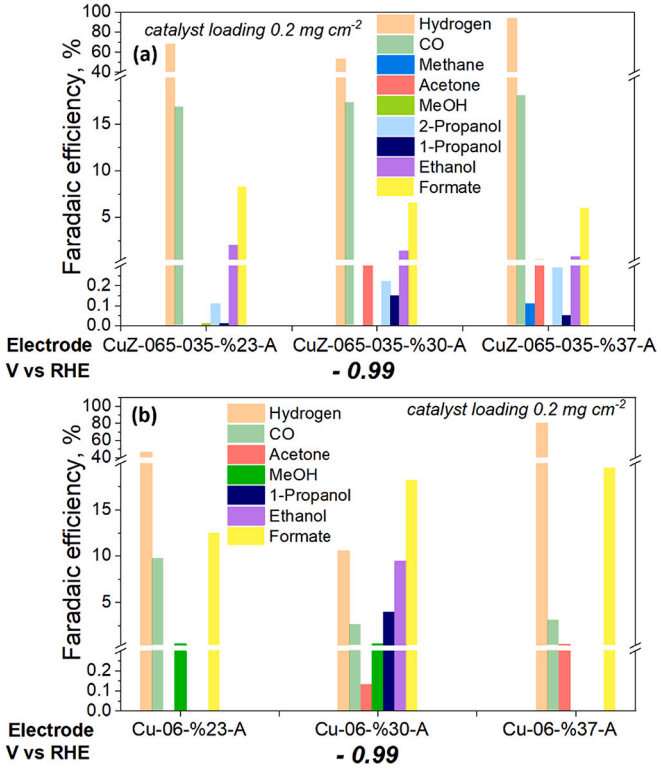

Fig. 13. Faradaic efficiencies for the US-prepared CuZ-06-035 (a) and US-prepared Cu-06 (b) catalysts with 0.2 mg cm^{-2}, tested in 1 M $KHCO_3$ aqueous electrolyte at −0.99 V vs RHE.

additional ohmic drop effects and render electrochemically inactive the catalytic sites inside the deeper pores [33]. In particular, slightly higher FEs were observed towards CO, H_2 and other liquid products like acetone and 2-propanol by increasing the applied US amplitude (Fig. 13 (a)). In this regard, it is possible to appreciate that the higher selectivity towards products more reduced than C_1 (i.e. 2-propanol) appears to correlate with the increase in the CO formation and decrease in the formate desorption. It has been demonstrated that the enriched ZnO surface increases the local CO concentration, allowing a higher formation of the *CO intermediate that is transformed by dimerisation reactions (that is, *CO-*CO or *CHx-*CO) into a C_{2+} product [12,40–42]. However, the small particles of US-prepared bicomponent CuZn materials promoted the syngas (CO + H_2) formation over the liquid products. Probably, the *CO intermediate does not stabilise enough on the small crystals and a high volume of pores of this material; therefore, the production rate of more reduced products is not favoured.

Regarding the US-synthesised CuO, Fig. 13(b) shows that the trend with respect to CO and formate production is the opposite. Higher FEs were observed towards formate production by increasing the applied US amplitude while the CO formation was suppressed. The best FE for alcohols (specially ethanol) were obtained by applying an amplitude of % 30. Interestingly, also in this case, the Cu-06-30%-A presents the lowest availability of electrocatalytic sites and high BET surface area. Then, it is demonstrated that the ohmic drop effects across the porous channels could play an important role in tuning the obtained products. Thus, the most promising catalyst for the liquid product among the new US-prepared catalysts is the Cu-06-%30-A with 14 % of FE to alcohols. For this reason, this catalyst was chosen for the rest of the investigations. We also observe that by increasing the applied amplitude, there is a clear trend favouring formate production.

3.2.2. *Effect of different Cu concentrations on electroactivity for EC CO_2R*

The electrocatalytic performance towards the CO_2 reduction reaction of a US-synthesised CuO-based catalyst prepared with a higher concentration of copper precursor was studied. The Cu-06-%30-A was added for comparison. These tests were carried out with 0.6 mg cm^{-2}. As shown in Fig. 14(a), increasing the copper nitrate concentration allowed a higher total current density with the new prepared Cu-1-%30-A catalyst. The reductive current density achieved ~ 40 mA cm^{-2}, slightly increasing by 5 % after 40 min. It is important to mention that both materials were subjected to the same pre-reduction treatment to reduce the CuO in the fresh electrode. In this regard, two hypotheses are proposed to explain the instability of the current density curve over time. On the one hand, the decreasing of the cathodic current density may be related to the bad transport of gaseous products through the catalytic layer at high reaction rates; instead, the increase may be ascribed to the continuing transformation of CuO to a more reduced species, which makes the electrode much more conductive. A better CO_2 reduction activity for alcohols was detected by increasing the concentration of the copper precursor (see Fig. 14 (b)). The Cu-1-%30-A catalyst increased 3-fold the FE (~ 11%) with about 4.2 mA cm^{-2} of partial current density towards alcohols. That behaviour could be due to the stabilisation of *CO species and subsequent dimerisation in higher pores volume made of a predominate size between 25 and 30 nm, as shown in Fig. 7(a). Additionally, according to the values shown in Table 3 for Cu-1-%30-A

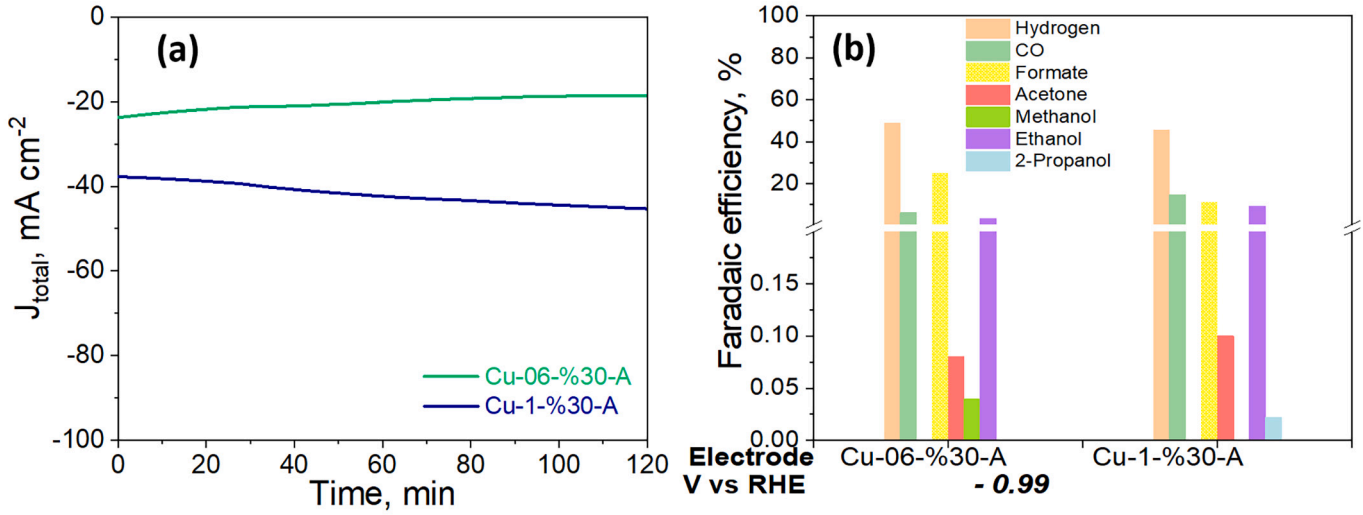

Fig. 14. Evolution time of the total current density of the electrochemical reduction of CO_2 (a) and Faradaic efficiencies (b) for Cu-06-%30-A and Cu-1-%30-A (0.6 mg cm^{-2}) tested in 1 M $KHCO_3$ aqueous electrolyte at −0.99 V vs RHE.

and Cu-06-%30-A, the higher the ECSA, the higher the geometric current density, which agrees with the results of Koper M. et al. [33] It seems that as the Cu precursor concentration increases, the electrocatalytic sites are more active; as well, it is plausible that the ohmic drop effects along the length of the porous channels are also decreased.

3.2.3. Effect of different precipitation times on electroactivity for EC CO_2R

The yields obtained for the synthesised catalysts with varying precipitation times are shown in Fig. 15. The Cu-06 catalysts were developed by assisting the synthesis with ultrasonic irradiation during different precipitation times at 30 % of applied amplitude.

As the precipitation time increases, an increase in the reductive current density was obtained, being that for 8 min and 12 min practically the same, as shown in Fig. 15(a). Contrary to what was previously observed, at higher precipitation times under US conditions, the lower the ECSA the higher the current density, which means that a longer US precipitation time induces a better specific activity (J_{ECSA}, mA cm$^{-2}_{ECSA}$) of the available catalytic sites. The highest obtained current density was ~30 mA cm^{-2}, which was stable for 60 min; then, it rose by 5 %. The CO_2 electrolysis results are presented in Fig. 15(b), where a marginal decrease in the production of alcohols can be appreciated by decreasing the precipitation time to 4 min. Instead, there are no greater differences between the 8P and 12P samples, with a partial current density of about −3.4 mA cm^{-2} to alcohols and > 40 % CO_2 reduction products. It is probably attributed to the fact that as the sonication time is increased, the overall cavitation effects in the system increase, which probably results in a better porous and crystalline structure (with crystallite size to 15 nm) that could promote the exposure of accessible active sites and facilitates the diffusion of CO_2 and products. Thus, a consequent improvement in C_{2+} products was observed [36,38,43–45].

3.2.4. Effect of calcination temperature on electroactivity for EC CO_2R

Copper oxide nanoparticles were prepared by assisting the ageing process with ultrasonic irradiation, with 0.6 M of a solution of copper nitrate as a starting precursor. The as-precipitated powders were calcined at various temperatures ranging from 250 to 550 °C. The results are shown in Fig. 16.

Fig. 16(a) shows small differences between the current density generated for the different calcined temperatures. The highest value was obtained at 250 °C and 350 °C (~30 mA cm^{-2}). Faradaic efficiencies for the different generated products can be appreciated in Fig. 16(b). The as-precipitated powders calcined at 350 °C present the most promising CO_2

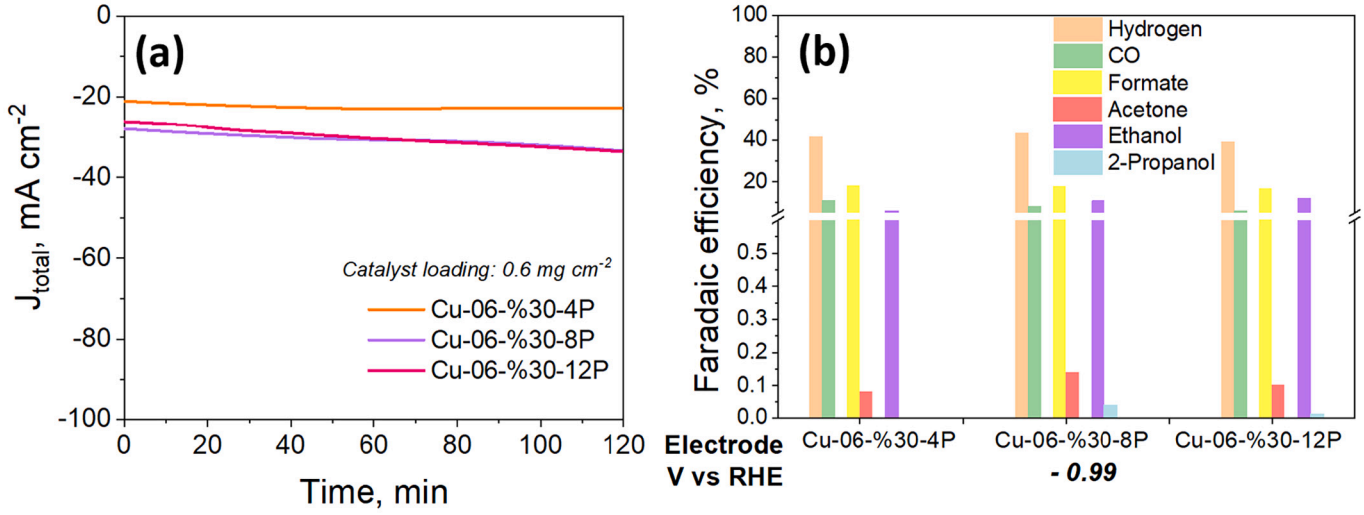

Fig. 15. Chronoamperometry responses of electrochemical reduction of CO_2 (a) and Faradaic efficiencies (b) for Cu-06-%30-XP. X stands for 4, 6 and 8 min. Tests were carried out with 0.6 mg cm^{-2} in 1 M $KHCO_3$ aqueous electrolyte at −0.99 V vs RHE.

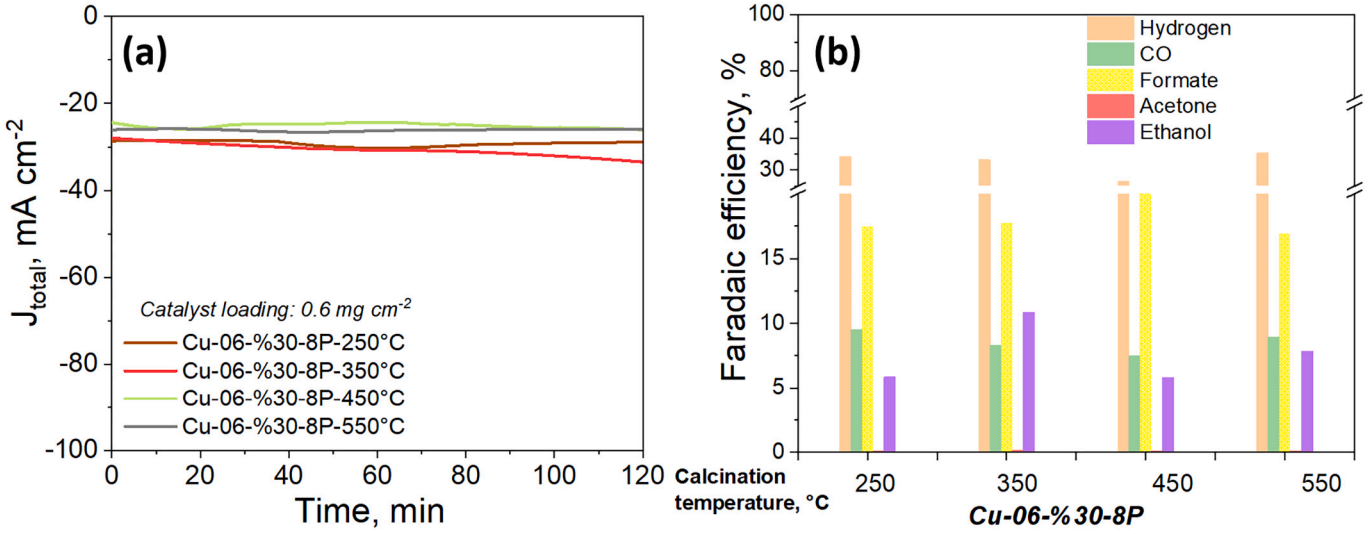

Fig. 16. Chronoamperometry responses of electrochemical reduction of CO_2 (a) and Faradaic efficiencies (b) for Cu-06-%30-8P calcined at different temperatures; 250, 350, 450 and 550 °C. Tests were carried out with 0.6 mg cm^{-2} in 1 M $KHCO_3$ aqueous electrolyte at −0.99 V vs RHE.

reduction electroactivity, achieving a total Faradaic efficiency towards C_{2+} products of ~ 11 %. It is worth noting that these products have > 95 % selectivity to ethanol. Usually, an increase in calcined temperature leads to obtaining larger crystallite sizes [26]. Here, the largest crystallites of 15 nm were obtained at 350 °C (see Table 3), and the smallest of 10 nm were obtained at 250 °C, which further confirms the role of crystal size on the performance of the catalysts. Further increasing calcined temperature up to 550 °C, the catalyst porosity drastically drops due to the effect of sintering occurring in the material (see Fig. 7 (b)), which probably hinders the electrocatalytic activity and the CO_2 diffusion. Indeed, increasing the calcination temperature diminishes the ECSA value, while increasing the mean pore size (see Fig. 7(c)), which further confirms that the pores size distribution influences the electrocatalyst activity.

3.2.5. *Influence of pore size on selectivity towards alcohols*

As mentioned before, the size of the pores of the catalysts influences selectivity. It is closely related to the CO retention time (RT) inside those pores, the *CO species stabilisation at the catalyst surface and their subsequent dimerisation to obtain more reduced products. Fig. 17 shows the FE towards alcohols with respect to pore size. Observing the points in the figures that correspond to groups whose tests were made with the same conditions, we can see that the blue curve evidences a trend. We observe that around 20–30 nm, there is an optimal value for pore size at which the highest FE towards alcohols was produced. Mostly ethanol, as mentioned previously. This point corresponds to the experiments done by varying the precipitation time under US conditions.

The existence of optimal pore size to produce alcohols is because certain conditions favour both the diffusion of CO_2 to the active sites of the catalyst where the reaction will evolve, as well as the adequate retention time of CO-species, enhancing the amount of *CO intermediate that can dimerise to obtain more reduced products. In Fig. 17, we also see that the efficiency towards alcohols is also very low for low pore sizes. That is probably because the diffusion of CO_2 and its conversion is limited. While for the pores larger than 20 nm, the limiting factor for obtaining alcohols is the faster diffusion and low retention time of gaseous CO, which does not allow the subsequent dimerisation of its adsorbed species. The Volcano-like plot of CO vs Ethanol productivity shown in Fig. 18 supports the previous hypotheses. The initial increase in the CO productivity is related to the samples with the lowest RT to CO in which the formation of the *CO intermediate is less favoured; thus, the optimal conditions for the *CO dimerisation are not presented and, consequently, there is low ethanol production. Then, the CO productivity decrease after a maximum value indicates an enhanced CO adsorption at the surface of the catalyst; i.e. an increased presence of bonded *CO species are available for its subsequent dimerisation and generation of products with more than one carbon-atom like ethanol, whose productivity is maximised in this region of the figure.

3.3. *Tested electrodes on a porous carbon support*

Two of the materials with the best performance for liquid products were selected to be tested in electrodes prepared on porous carbon supports: i.e. Cu-1-%30-A and Cu-06-%30-8P; to reduce the issue of bubbles accumulation on the catalyst surface. In the case of the Cu-1-%30-A, an increase in the current density (~-42 mA cm^{-2} with respect to

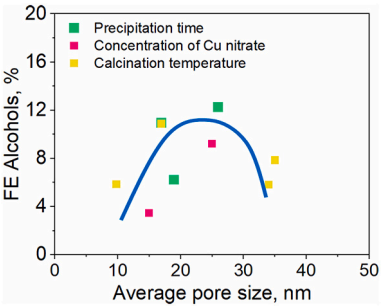

Fig. 17. Relationship between FE alcohols and pore size for different groups of catalysts.

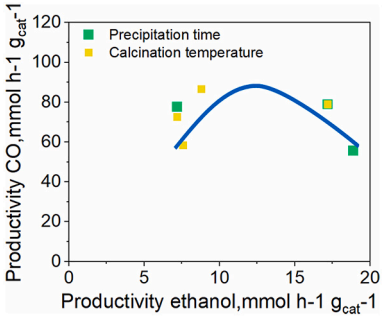

Fig. 18. Relationship between productivity towards ethanol and towards CO.

~-20 mA cm^{-2} for Cu-06-%30-A) was obtained by increasing the concentration of the precursor, in addition to a better CO_2 reduction activity for alcohols in the RDE system. However, the response obtained in the reduction of CO_2 was slightly unstable. As mentioned above, this can be attributed to the bad transport of gaseous products in the catalytic layer. On the other hand, the Cu-06-%30-8P tested in the RDE system presented a relevant current density (~-31 mA cm^{-2}) in the CO_2 reduction and a notable selectivity towards alcohols, especially towards ethanol. However, it also presented instability during the CO_2 reduction reaction. The tests carried out in RDE have the disadvantage that the glassy carbon surface is non-porous, which could generate bubbles accumulationthat reduces the availability of the active sites. A way to solve the difficulty in handling the gaseous products through the pores of the catalytic layer is to deposit the catalytic ink on a porous conductive substrate. Some advantages of the carbon-based porous substrate are the high specific surface area, high electrical conductivity, and low cost [46]. For comparison purposes, the porous electrodes were tested under the galvanostatic condition at the same current densities achieved during the RDE test for each specific catalyst. The chronopotentiometry responses are shown in Fig. S4 in the Supporting Information.

The physicochemical characterisation of the electrodes, fresh and tested, was done through FESEM to study the changes that occur to the catalytic layer during the testing phase. Fig. 19 compares the FESEM images before and after the test for both catalysts.

In terms of morphology, changes were observed between the electrode before and after the test. However, it should be noted that in Fig. 6 and Fig. 8, the FESEM images correspond only to the powders. In contrast, in Fig. 19 (a,c), they correspond to the fresh electrodes, in which the particles have been deposited immersed in a solution of Nafion and isopropanol for the ink preparation. For this reason, Fig. 19 shows that a film of this polymeric material covers the particles. In Fig. 19 (a), the morphology of the Cu-1-%30-A catalyst in the electrode is observed, and it is similar to that shown in Fig. 6 (b). There is an incomplete formation of CuO that does not allow to complete the spherical shape of the particles. Fig. 19 (b) shows that the micrometric catalyst particles are covered with much smaller particles after the electrochemical reaction. Regarding the Cu-06-% 30-8P electrode, in Fig. 19(c), the particles are not modified with respect to the powders. After the test, in Fig. 19(d), they appear much smaller, less defined, and with greater dispersion.

Fig. 20 shows the selectivity towards CO_2 reduction products obtained with the porous carbon electrodes, neglecting hydrogen production.

The results show that the same CO_2 reduction products observed in the RDE experiments were obtained with the catalyst deposited in the porous carbon supports. The Cu-06-%30-8P catalyst has a higher selectivity towards alcohols, which agrees with the results shown in section 3.2.5, in which the influence of pore size and selectivity towards alcohols was studied. The sample synthesised by applying the US during the precipitation time had better physical characteristics with respect to the sample prepared with the highest concentration of the nitrate precursor. As shown in Fig. 7 and Table 3, the Cu-06-%30-8P sample has a higher surface area (~32 m^2 g^{-1}) and narrower distribution of optimum pores sizes (~ 20 nm) that allows reaching a selectivity of 59% towards alcohols. Instead, the selectivity towards formate does not appear to have been highly influenced, while CO is 4.8-fold higher for the Cu-1-% 30-A sample. Having these two fresh samples a similar crystalline CuO phase, in the latter, there was probably a lower stabilisation of the *CO

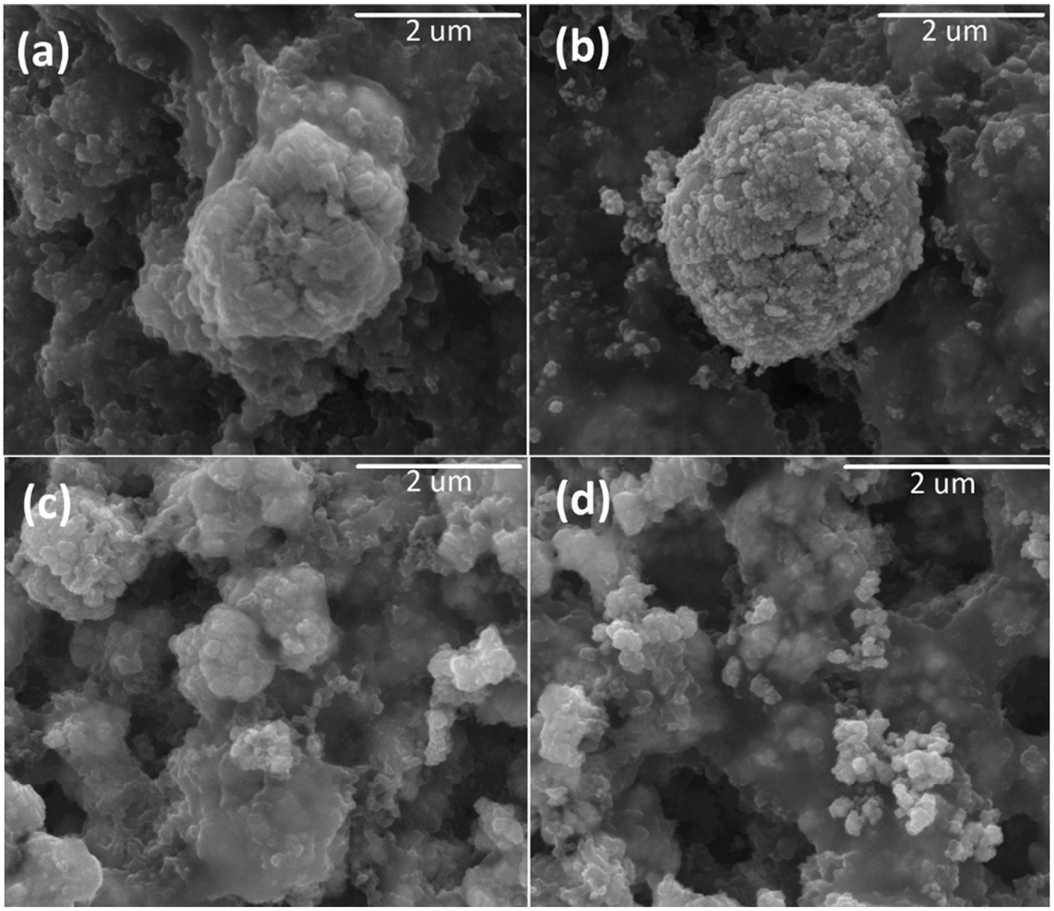

Fig. 19. FESEM micrographs of the electrodes on porous carbon support (a) Cu-1-%30-A Fresh, (b) Cu-1-%30-A Tested, (c) Cu-06-%30-8P Fresh, and (d) Cu-06-%30-8P Tested.

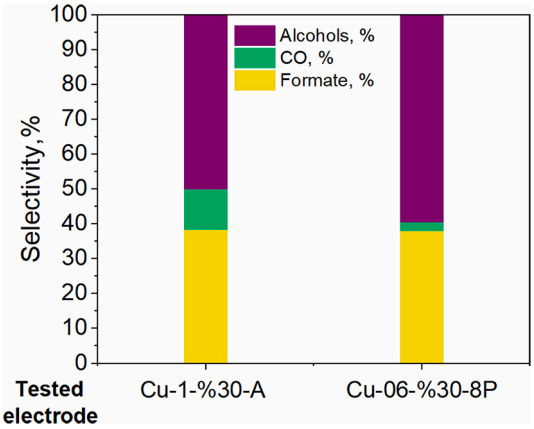

Fig. 20. Faradaic efficiencies of the porous carbon-supported electrode. Tests were carried out with 0.6 mg cm^{-2} in 1 M $KHCO_3$ aqueous electrolyte.

intermediate due to the bigger pores size, which induced a greater amount of produced CO and a lower selectivity towards alcohols.

4. Conclusions

In this work new catalysts were developed by assisting the co-precipitation synthesis with ultrasonic irradiation. The effect of the ultrasounds was evaluated in the precipitation time and the ageing process.

During the CO_2 electro reduction tests in aqueous media, enhanced selectivity towards H_2 and C_1 products (CO and formate) was obtained with the CuZ catalysts, which were synthesised with the ageing process under ultrasound irradiation. An improved synergistic effect between the ZnO and CuO metal oxides has been demonstrated towards these products with respect to the original CuZ catalyst. Under the same operating conditions, the US-prepared CuZ catalysts increased the productivity of syngas by $>\sim$1.4-fold. It could be explained by the influence of the use of ultrasound to promote the dispersion of very fine and uniform CuO particles (crystallite sizes <7 nm). Besides, new CuO crystalline planes were promoted by applying different US amplitude percentages. On the other hand, the BET surface area increased by 100 % with respect to the original sample in most of the US-assisted CuO synthesis under different amplitudes, obtaining > 14 % of FE to alcohols in the RDE system with a catalyst loading of 0.2 mg cm^{-2}. Additionally, the effects of precursor concentration, US-assisted precipitation time, and calcination temperature of the as-synthesised powders on the electroactivity performance of the catalysts were discussed. It was possible to tune the physical and chemical properties of the synthesised nanoparticles through these changes. Mesoporous materials with mean pores size of around 20 were formed, which induced better CO_2 adsorption and diffusion, and this allows to have the optimal conditions for increasing the CO retention time in the catalyst pores and enhancing both the formation of *CO intermediates and its dimerisation to produce products with more than one carbon atom. Two catalysts with interesting results were selected for their deposition on a porous carbon substrate. It was observed that the same CO_2 reduction products were produced with respect to the RDE test, and it was possible to validate the relationship between pore size and selectivity towards alcohols. In conclusion, the electrocatalytic activity for the CO_2 reduction reaction to alcohols was improved by increasing the copper precursor concentration (up to 1 M) and increasing the precipitation time (up to 8–12 min). Considering that liquid products from the electrochemical CO_2 reduction have advantages in terms of transportation, storage, and handling, the most promising electrocatalysts were able to produce a total cathodic current density higher than 10 mA cm^{-2} and FE towards liquid products ($>C_{1+}$) of $\sim$20 % in this liquid-phase system. Further investigations are needed to pursue high current densities (> 200 mA cm^{-2}) and industrially relevant production rates. Furthermore, superficial characterisations and advanced analysis under operative conditions are necessary to understand the role of the ultrasound in the CuO-formed species for the EC CO_2R.

CRediT authorship contribution statement

Hilmar Guzmán: Methodology, Validation, Formal analysis, Investigation, Writing – original draft, Writing – review & editing. **Daniela Roldán:** Validation, Investigation, Writing – review & editing. **Nunzio Russo:** Resources, Writing – review & editing. **Simelys Hernández:** Conceptualization, Formal analysis, Funding acquisition, Resources, Supervision, Writing – review & editing.

Declaration of Competing Interest

The authors declare the following financial interests/personal relationships which may be considered as potential competing interests:

Simelys Hernández reports financial support was provided by Eni SpA and Fondazione Compagnia di San Paolo.

Acknowledgements

This work has been performed with the financial support of Eni SpA: R&D Program Energy Transition (Cattura e Utilizzo CO2) - and of the project CO2Synthesis (ID ROL: 67910) funded by Fondazione Compagnia di San Paolo in the Call Trapezio - Linea 1.

Appendix A. Supplementary data

Supplementary data to this article can be found online at https://doi.org/10.1016/j.susmat.2022.e00557.

References

[1] IEA, Global Energy Review: CO_2 Emissions in 2020, IEA, Paris, (2020). https://www.iea.org/articles/global-energy-review-co2-emissions-in-2020, 2021 (accessed July 2, 2022).
[2] J. Albo, A. Irabien, Cu_2O-loaded gas diffusion electrodes for the continuous electrochemical reduction of CO_2 to methanol, J. Catal. 343 (2016) 232–239, https://doi.org/10.1016/j.jcat.2015.11.014.
[3] N. Gutiérrez-Guerra, L. Moreno-López, J.C. Serrano-Ruiz, J.L. Valverde, A. de Lucas-Consuegra, Gas phase electrocatalytic conversion of CO_2 to syn-fuels on Cu based catalysts-electrodes, Appl. Catal. B Environ. 188 (2016) 272–282, https://doi.org/10.1016/j.apcatb.2016.02.010.
[4] M. Jouny, W. Luc, F. Jiao, General techno-economic analysis of CO_2 electrolysis systems, Ind. Eng. Chem. Res. 57 (2018) 2165–2177, https://doi.org/10.1021/acs.iecr.7b03514.
[5] S. Mou, Y. Li, L. Yue, J. Liang, Y. Luo, Q. Liu, T. Li, S. Lu, A.M. Asiri, X. Xiong, D. Ma, X. Sun, Cu_2Sb decorated Cu nanowire arrays for selective electrocatalytic CO_2 to CO conversion, Nano Res. 14 (2021) 2831–2836, https://doi.org/10.1007/s12274-021-3295-1.
[6] X. Jiang, X. Wang, Q. Wang, X. Xiao, J. Chen, M. Wang, Y. Shen, Efficient activation and electroreduction of carbon dioxide on an electrocatalyst cadmium carbonate, ACS Appl. Energy Mater. 4 (2021) 2073–2080, https://doi.org/10.1021/acsaem.0c02267.
[7] H. Guzmán, N. Russo, S. Hernández, CO_2 valorisation towards alcohols by Cu-based electrocatalysts: challenges and perspectives, Green Chem. 23 (2021) 1896–1920, https://doi.org/10.1039/D0GC03334K.
[8] H. Guzmán, F. Salomone, E. Batuecas, T. Tommasi, N. Russo, S. Bensaid, S. Hernández, How to make sustainable CO_2 conversion to methanol: thermocatalytic versus electrocatalytic technology, Chem. Eng. J. 417 (2021), 127973, https://doi.org/10.1016/j.cej.2020.127973.
[9] Y.Y. Birdja, E. Pérez-Gallent, M.C. Figueiredo, A.J. Göttle, F. Calle-Vallejo, M.T. M. Koper, Advances and challenges in understanding the electrocatalytic conversion of carbon dioxide to fuels, Nat. Energy 4 (2019) 732–745, https://doi.org/10.1038/s41560-019-0450-y.
[10] L. Ji, X. Li, Y. Zhang, S. Mou, T. Wu, Q. Liu, B. Li, X. Zhu, Y. Luo, X. Shi, A.M. Asiri, X. Sun, Highly selective electrochemical reduction of CO_2 to alcohols on an FeP nanoarray, Ngew. Chem. 132 (2020) 768–772, https://doi.org/10.1002/anie.201912836.
[11] H. Guzmán, N. Russo, S. Hernández, CO_2 valorisation towards alcohols by cu-based electrocatalysts: challenges and perspectives, Green Chem. 23 (2021) 1896–1920, https://doi.org/10.1039/D0GC03334K.

[12] H. Guzmán, F. Salomone, S. Bensaid, M. Castellino, N. Russo, S. Hernández, CO_2 conversion to alcohols over cu/ZnO catalysts: prospective synergies between electrocatalytic and thermocatalytic routes, ACS Appl. Mater. Interfaces 14 (2022) 517–530, https://doi.org/10.1021/acsami.1c15871.
[13] H. Guzmán, N. Russo, S. Hernández, CO_2 valorisation towards alcohols by cu-based electrocatalysts: challenges and perspectives, Green Chem. 23 (2021) 1896–1920, https://doi.org/10.1039/D0GC03334K.
[14] W.M. Rangel, R.A.A. Boca Santa, H.G. Riella, A facile method for synthesis of nanostructured copper (II) oxide by coprecipitation, J. Mater. Res. Technol. 9 (2020) 994–1004, https://doi.org/10.1016/j.jmrt.2019.11.039.
[15] M. Vijayakumar, Development of Rare Earth Based Lithium Silicates and Nanocomposite Polymer Solid Electrolytes for Lithium Battery Applications, 2012, p. 162.
[16] R. Singh Yadav, I. Kuřitka, J. Vilcakova, T. Jamatia, M. Machovsky, D. Skoda, P. Urbánek, M. Masař, M. Urbánek, L. Kalina, J. Havlica, Impact of sonochemical synthesis condition on the structural and physical properties of $MnFe_2O_4$ spinel ferrite nanoparticles, Ultrason. Sonochem. 61 (2020), https://doi.org/10.1016/j.ultsonch.2019.104839.
[17] V. Jafari, A. Allahverdi, M. Vafaei, Ultrasound-assisted synthesis of colloidal nanosilica from silica fume: effect of sonication time on the properties of product, Adv. Powder Technol. 25 (2014) 1571–1577, https://doi.org/10.1016/j.apt.2014.05.011.
[18] S. Allahyari, M. Haghighi, A. Ebadi, S. Hosseinzadeh, Effect of irradiation power and time on ultrasound assisted co-precipitation of nanostructured CuO-ZnO-Al_2O_2 over HZSM-5 used for direct conversion of syngas to DME as a green fuel, Energy Convers. Manag. 83 (2014) 212–222, https://doi.org/10.1016/j.enconman.2014.03.071.
[19] M.D. Luque de Castro, F. Priego-Capote, Ultrasound-assisted crystallization (sonocrystallization), Ultrason. Sonochem. 14 (2007) 717–724, https://doi.org/10.1016/j.ultsonch.2006.12.004.
[20] S. Allahyari, M. Haghighi, A. Ebadi, S. Hosseinzadeh, Effect of irradiation power and time on ultrasound assisted co-precipitation of nanostructured CuO-ZnO-Al_2O_2 over HZSM-5 used for direct conversion of syngas to DME as a green fuel, Energy Convers. Manag. 83 (2014) 212–222, https://doi.org/10.1016/j.enconman.2014.03.071.
[21] Y.H. Yap, M.S.W. Lim, Z.Y. Lee, K.C. Lai, M.A. Jamaal, F.H. Wong, H.K. Ng, S. S. Lim, T.J. Tiong, Effects of sonication on co-precipitation synthesis and activity of copper manganese oxide catalyst to remove methane and sulphur dioxide gases, Ultrason. Sonochem. 40 (2018) 57–67, https://doi.org/10.1016/j.ultsonch.2017.06.032.
[22] V.D.B.C. Dasireddy, B. Likozar, The role of copper oxidation state in cu/ZnO/Al_2O_3 catalysts in CO_2 hydrogenation and methanol productivity, Renew. Energy 140 (2019) 452–460, https://doi.org/10.1016/j.renene.2019.03.073.
[23] D.V. Pinjari, K. Prasad, P.R. Gogate, S.T. Mhaske, A.B. Pandit, Synthesis of titanium dioxide by ultrasound assisted sol-gel technique: effect of calcination and sonication time, Ultrason. Sonochem. 23 (2015) 185–191, https://doi.org/10.1016/j.ultsonch.2014.10.017.
[24] K. Ohta, K. Suda, S. Kaneco, T. Mizuno, Electrochemical reduction of carbon dioxide at Cu electrode under ultrasonic irradiation, J. Electrochem. Soc. 147 (2000) 233, https://doi.org/10.1149/1.1393180.
[25] M.H. Islam, H. Mehrabi, R.H. Coridan, O.S. Burheim, J.Y. Hihn, B.G. Pollet, The effects of power ultrasound (24 kHz) on the electrochemical reduction of CO_2 on polycrystalline copper electrodes, Ultrason. Sonochem. 72 (2021), 105401, https://doi.org/10.1016/j.ultsonch.2020.105401.
[26] N. Wongpisutpaisan, P. Charoonsuk, N. Vittayakorn, W. Pecharapa, Sonochemical synthesis and characterization of copper oxide nanoparticles, Energy Procedia 9 (2011) 404–409, https://doi.org/10.1016/j.egypro.2011.09.044.
[27] R. Zhao, P. Ding, P. Wei, L. Zhang, Q. Liu, Y. Luo, T. Li, S. Lu, X. Shi, S. Gao, A. M. Asiri, Z. Wang, X. Sun, Recent progress in electrocatalytic methanation of CO_2 at ambient conditions, Adv. Funct. Mater. 31 (2021), https://doi.org/10.1002/adfm.202009449.
[28] C. Baltes, S. Vukojević, F. Schüth, Correlations between synthesis, precursor, and catalyst structure and activity of a large set of CuO/ZnO/Al_2O_3 catalysts for methanol synthesis, J. Catal. 258 (2008) 334–344, https://doi.org/10.1016/j.jcat.2008.07.004.
[29] H. Guzmán, D. Roldán, A. Sacco, M. Castellino, M. Fontana, N. Russo, S. Hernández, CuZnAl-oxide nanopyramidal mesoporous materials for the electrocatalytic CO_2 reduction to syngas: tuning of H_2/CO ratio, Nanomaterials. 11 (2021) 3052, https://doi.org/10.3390/nano11113052.
[30] S. Allahyari, M. Haghighi, A. Ebadi, S. Hosseinzadeh, Ultrasound assisted co-precipitation of nanostructured CuO–ZnO–Al_2O_3 over HZSM-5: effect of precursor and irradiation power on nanocatalyst properties and catalytic performance for direct syngas to DME, Ultrason. Sonochem. 21 (2014) 663–673, https://doi.org/10.1016/j.ultsonch.2013.09.014.
[31] H. Ataee-Esfahani, L. Wang, Y. Nemoto, Y. Yamauchi, Synthesis of bimetallic Au@Pt nanoparticles with Au core and nanostructured Pt shell toward highly active electrocatalysts, Chem. Mater. 22 (2010) 6310–6318, https://doi.org/10.1021/cm102074w.
[32] J.H. Jang, J. Kim, Y.H. Lee, I.Y. Kim, M.H. Park, C.W. Yang, S.J. Hwang, Y. U. Kwon, One-pot synthesis of core-shell-like Pt_3Co nanoparticle electrocatalyst with Pt-enriched surface for oxygen reduction reaction in fuel cells, Energy Environ. Sci. 4 (2011) 4947–4953, https://doi.org/10.1039/c1ee01825f.
[33] A. Goyal, C.J. Bondue, M. Graf, M.T.M. Koper, Effect of pore diameter and length on electrochemical CO_2 reduction reaction at nanoporous gold catalysts, Chem. Sci. 13 (2022) 3288–3298, https://doi.org/10.1039/d1sc05743j.
[34] D. Gao, R.M. Arán-Ais, H.S. Jeon, B. Roldan Cuenya, Rational catalyst and electrolyte design for CO_2 electroreduction towards multicarbon products, Nat. Catal. 2 (2019) 198–210, https://doi.org/10.1038/s41929-019-0235-5.
[35] B.C. Marepally, C. Ampelli, C. Genovese, F. Tavella, L. Veyre, E.A. Quadrelli, S. Perathoner, G. Centi, Role of small Cu nanoparticles in the behaviour of nanocarbon-based electrodes for the electrocatalytic reduction of CO_2, J. CO2 Utiliz. 21 (2017) 534–542, https://doi.org/10.1016/j.jcou.2017.08.008.
[36] J.J. Velasco-Vélez, T. Jones, D. Gao, E. Carbonio, R. Arrigo, C.J. Hsu, Y.C. Huang, C.L. Dong, J.M. Chen, J.F. Lee, P. Strasser, B. Roldan Cuenya, R. Schlögl, A. Knop-Gericke, C.H. Chuang, The role of the copper oxidation state in the electrocatalytic reduction of CO_2 into valuable hydrocarbons, ACS Sustain. Chem. Eng. 7 (2019) 1485–1492, https://doi.org/10.1021/acssuschemeng.8b05106.
[37] A. Karelovic, P. Ruiz, The role of copper particle size in low pressure methanol synthesis via CO_2 hydrogenation over Cu/ZnO catalysts, Catal. Sci. Technol. 5 (2015) 869–881, https://doi.org/10.1039/c4cy00848k.
[38] F. Arena, K. Barbera, G. Italiano, G. Bonura, L. Spadaro, F. Frusteri, Synthesis, characterization and activity pattern of Cu – ZnO/ZrO_2 catalysts in the hydrogenation of carbon dioxide to methanol, J. Catal. 249 (2007) 185–194, https://doi.org/10.1016/j.jcat.2007.04.003.
[39] I. Hjorth, M. Nord, M. Rønning, J. Yang, D. Chen, Electrochemical reduction of CO_2 to synthesis gas on CNT supported $Cu_xZn_{1-x}O$ catalysts, Catal. Today 357 (2020) 311–321, https://doi.org/10.1016/j.cattod.2019.02.045.
[40] H. Xiao, W.A. Goddard, T. Cheng, Y. Liu, Cu metal embedded in oxidized matrix catalyst to promote CO_2 activation and CO dimerization for electrochemical reduction of CO_2, Proc. Natl. Acad. Sci. U. S. A. 114 (2017) 6685–6688, https://doi.org/10.1073/pnas.1702405114.
[41] S.B. Varandili, D. Stoian, J. Vavra, K. Rossi, J.R. Pankhurst, Y.T. Guntern, N. López, R. Buonsanti, Elucidating the structure-dependent selectivity of CuZn towards methane and ethanol in CO_2 electroreduction using tailored Cu/ZnO precatalysts, Chem. Sci. (2021), https://doi.org/10.1039/d1sc04271h.
[42] P. Iyengar, M.J. Kolb, J.R. Pankhurst, F. Calle-Vallejo, R. Buonsanti, Elucidating the facet-dependent selectivity for CO_2 Electroreduction to ethanol of Cu-Ag tandem catalysts, ACS Catal. 11 (2021) 4456–4463, https://doi.org/10.1021/acscatal.1c00420.
[43] D. Gao, R.M. Arán-Ais, H.S. Jeon, B. Roldan Cuenya, Rational catalyst and electrolyte design for CO_2 electroreduction towards multicarbon products, Nau. Catal. 2 (2019) 198–210, https://doi.org/10.1038/s41929-019-0235-5.
[44] B.C. Marepally, C. Ampelli, C. Genovese, F. Tavella, L. Veyre, E.A. Quadrelli, S. Perathoner, G. Centi, Role of small Cu nanoparticles in the behaviour of nanocarbon-based electrodes for the electrocatalytic reduction of CO_2, J. CO2 Utiliz. 21 (2017) 534–542, https://doi.org/10.1016/j.jcou.2017.08.008.
[45] I. Hjorth, M. Nord, M. Rønning, J. Yang, D. Chen, Electrochemical reduction of CO_2 to synthesis gas on CNT supported $Cu_xZn_{1-x}O$ catalysts, Catal. Today 357 (2020) 311–321, https://doi.org/10.1016/j.cattod.2019.02.045.
[46] H.M. Luo, H. Chen, Y.Z. Chen, P. Li, J.Q. Zhang, X. Zhao, Simple synthesis of porous carbon materials for high-performance supercapacitors, J. Appl. Electrochem. 46 (2016) 703–712, https://doi.org/10.1007/s10800-016-0958-9.